### Title

MiR-690 treatment causes decreased fibrosis and steatosis and restores specific Kupffer cell functions in NASH




### Journal

Cell Metabolism, 34(7)

### ISSN

1550-4131



### Authors

Gao, Hong
Jin, Zhongmou
Bandyopadhyay, Gautam
et al.



### Publication Date

2022-07-01

### DOI

10.1016/j.cmet.2022.05.008

Cell Metabolism

Article

# MiR-690 treatment causes decreased fibrosis and steatosis and restores specific Kupffer cell functions in NASH

## Graphical abstract

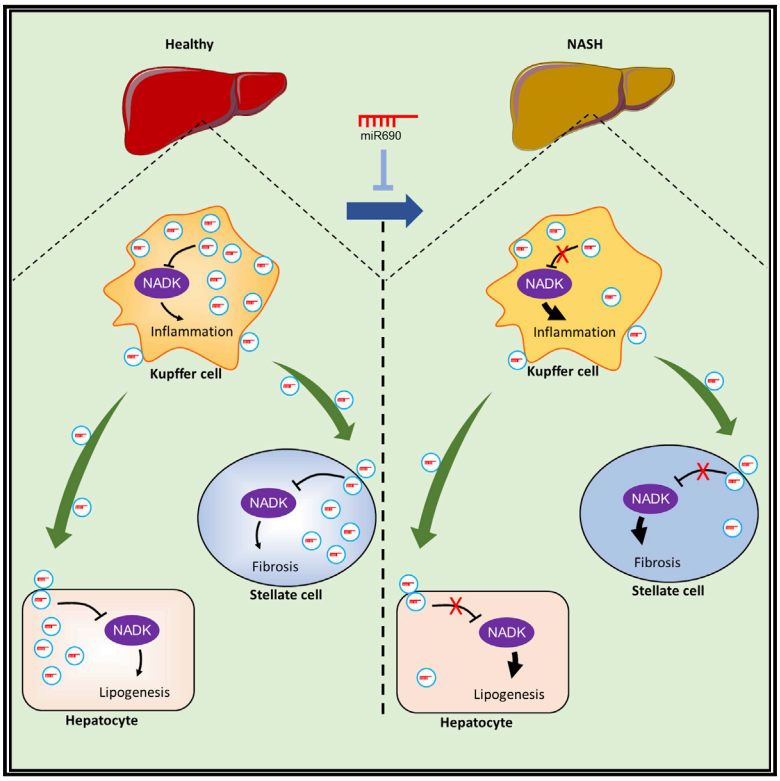


## Highlights

- miR-690 treatment blunts liver fibrosis, inflammation, and steatosis
- miR-690 is a key mediator of normal KC function
- KCs are the main source of miR-690 for other liver cells
- miR-690-*Nadk* axis regulates lipogenesis and fibrogenesis in SCs

## Authors

Hong Gao, Zhongmou Jin, Gautam Bandyopadhyay, ..., David A. Brenner, Wei Ying, Jerrold M. Olefsky

## Correspondence

weying@health.ucsd.edu (W.Y.), jolefsky@health.ucsd.edu (J.M.O.)

## In brief

Gao et al. report that Kupffer cell-derived exosomal miRNA-690 directly inhibits fibrogenesis, *de novo* lipogenesis, and inflammation *in vitro* and prevents the development of nonalcoholic steatohepatitis (NASH) in mice fed a Western diet.

Gao et al., 2022, Cell Metabolism *34*, 1–13
August 2, 2022 
https://doi.org/10.1016/j.cmet.2022.05.008

CellPress

Cell Metabolism

CellPress

Article

# MiR-690 treatment causes decreased fibrosis and steatosis and restores specific Kupffer cell functions in NASH

Hong Gao,[1] Zhongmou Jin,[2] Gautam Bandyopadhyay,[1] Karina Cunha e Rocha,[1] Xiao Liu,[3,4] Huayi Zhao,[3] Dinghong Zhang,[1] Hani Jouihan,[5] Soheil Pourshahian,[6] Tatiana Kisseleva,[4] David A. Brenner,[3] Wei Ying,[1,*] and Jerrold M. Olefsky[1,7,*]

[1]Division of Endocrinology & Metabolism, Department of Medicine, University of California, San Diego, La Jolla, CA 92093, USA
[2]Division of Biological Sciences, University of California, San Diego, La Jolla, CA 92093, USA
[3]Department of Medicine, University of California, San Diego, La Jolla, CA 92093, USA
[4]Department of Surgery, University of California, San Diego, La Jolla, CA 92093, USA
[5]Janssen Research & Development, Janssen Pharmaceutical Companies of Johnson & Johnson, Spring House, PA 19477, USA
[6]Janssen Pharmaceutical Companies of Johnson & Johnson, San Francisco, CA 94080, USA
[7]Lead contact
*Correspondence: weying@health.ucsd.edu (W.Y.), jolefsky@health.ucsd.edu (J.M.O.)
https://doi.org/10.1016/j.cmet.2022.05.008

## SUMMARY

Nonalcoholic steatohepatitis (NASH) is a liver disease associated with significant morbidity. Kupffer cells (KCs) produce endogenous miR-690 and, via exosome secretion, shuttle this miRNA to other liver cells, such as hepatocytes, recruited hepatic macrophages (RHMs), and hepatic stellate cells (HSCs). miR-690 directly inhibits fibrogenesis in HSCs, inflammation in RHMs, and *de novo* lipogenesis in hepatocytes. When an miR-690 mimic is administered to NASH mice *in vivo*, all the features of the NASH phenotype are robustly inhibited. During the development of NASH, KCs become miR-690 deficient, and miR-690 levels are markedly lower in mouse and human NASH livers than in controls. KC-specific KO of miR-690 promotes NASH pathogenesis. A primary target of miR-690 is NADK mRNA, and NADK levels are inversely proportional to the cellular miR-690 content. These studies show that KCs play a central role in the etiology of NASH and raise the possibility that miR-690 could emerge as a therapeutic for this condition.

## INTRODUCTION

Obesity and nonalcoholic fatty liver disease (NAFLD) are closely intertwined. Due to the epidemic of obesity, the prevalence of NAFLD has risen rapidly with an estimated worldwide prevalence of ~20%. About 30% of patients with NAFLD develop nonalcoholic steatohepatitis (NASH), which includes steatosis, inflammation, and fibrosis (Kazankov et al., 2019; Sheka et al., 2020; Yu et al., 2013). NASH is emerging as one of the most common liver diseases and is now recognized as a major cause of cirrhosis, liver failure, and hepatocellular cancer and a leading cause of liver transplantation (Anstee et al., 2013; Noureddin et al., 2018). Although there are many concepts on the mechanisms that underly the development of NASH and its progression (Friedman et al., 2018; Lee and Friedman, 2022; Tabas and Glass, 2013; Tacke, 2017; Wesolowski et al., 2017; Zhu et al., 2021), a full understanding of the disease pathogenesis is unknown and the development of effective drugs is still elusive.

Exosomes are nanoparticles secreted by all cell types. They enter the extracellular tissue space and ultimately the circulation and provide a vehicle for intercellular and intra-organ communication (Isaac et al., 2021; Tkach and Théry, 2016). Exosomes contain a variety of cargoes, and exosomal miRNAs are key components that mediate many of the functional effects of exosomes and can also serve as disease biomarkers (Alexander et al., 2015; Isaac et al., 2021). Our previous studies showed that miR-690-containing exosomes secreted by M2 bone marrow-derived macrophages (BMDMs) exert potent insulin-sensitizing effects (Ying et al., 2021). Due to the close relationship between NASH and insulin resistance, we postulated that M2 BMDM-derived exosomes and miR-690 mimics could improve NASH.

Here, we show that nanoparticles containing an miR-690 mimic can directly reduce fibrosis and inflammation in two NASH models. First, the miR-690 mimic inhibited fibrogenic gene expression in cultured liver spheroids incubated in a NASH-inducing cocktail. Second, the miR-690 mimic markedly reduced all the major features of NASH, including fibrosis, steatosis, and inflammation in Western diet (WD)-fed NASH mice. Importantly, normal Kupffer cells (KCs) express high levels of endogenous miR-690 and locally shuttle this miRNA through secreted exosomes to other nearby liver cells such as hepatocytes and hepatic stellate cells (HSCs). miR-690 levels are markedly reduced in NASH KCs, leading to a corresponding reduction

Please cite this article in press as: Gao et al., MiR-690 treatment causes decreased fibrosis and steatosis and restores specific Kupffer cell functions in NASH, Cell Metabolism (2022), https://doi.org/10.1016/j.cmet.2022.05.008



in miR-690 in hepatocytes and HSCs, directly contributing to the development of the NASH phenotype. As a result of the decline in miR-690 content, NASH KCs display impaired phagocytic efficiency and can promote insulin resistance in hepatocytes and activate the fibrogenic program in HSCs. These dysfunctional aspects of NASH KCs are completely reversed by exogenous treatment with an miR-690 mimic. Finally, the major mRNA target of miR-690 is NADK and NADK levels are increased in NASH liver cells, whereas $NAD^+$ levels are repressed. Replacement of $NAD^+$ recapitulates the beneficial effects of miR-690 treatment. Thus, miR-690 holds the potential as a future treatment for NASH.

## RESULTS

### Effects of miR-690 on liver spheroids

We have previously shown that exosomal miR-690 has robust effects to improve insulin sensitivity *in vitro* in adipocytes, hepatocytes, and skeletal muscle cells, as well as *in vivo* when administered to insulin-resistant mice (Ying et al., 2021). Since most patients with NASH are obese and/or insulin resistant, this prompted us to hypothesize that treatment with miR-690 could have beneficial effects to interrupt the NASH phenotype. To initially assess this idea, we generated a liver spheroid system by mixing primary hepatocytes, nonparenchymal cells (NPCs), and HSCs obtained from normal mouse livers (Broutier et al., 2016; Elbadawy et al., 2020; McCarron et al., 2021; Prior et al., 2019). When cultured together over a 14-day period, these cells develop into spheroidal-shaped liver spheroids in 24-well ultra-low adhesion plates (Figure S1A). Compared with long-term incubation of primary hepatocytes alone, the liver spheroids with multiple cell types expressed much greater levels of fibrogenic and inflammatory genes (Figure S1B). To further approximate the NASH process, we treated these liver spheroids with a mixture of fatty acids (FAs), fructose, and lipopolysaccharide (LPS); this cocktail further activates the fibrogenic and inflammatory phenotype (Figure S1B).

To directly assess the role of miR-690 in this system, we treated these liver spheroids with an miR-690 mimic encapsulated in artificial liposomes at days 5, 8, and 11 during the culture period and then analyzed the results at the end of 14 days. As seen in Figure 1A, miR-690 treatment substantially reduced the expression levels of a variety of fibrogenic genes, whereas expression of *Bambi*, a gene associated with the inactive or quiescent SCs, increased. In addition, miR-690 treatment reduced protein levels of collagen I and TIMP1 in these spheroids but was without effect on spheroids containing only hepatocytes (Figures S1C and S1D). To determine how these effects translated to a human system, we prepared liver spheroids using human hepatocytes, NPCs, and HSCs. As in the mouse spheroid system, the combination of FA, LPS, and fructose stimulated fibrogenesis and inflammation. Treatment with the miR-690 mimic produced a 2- to 3-fold increase in miR-690 levels in these spheroids and repressed fibrogenic and inflammatory gene and protein expression (Figures 1B and S1E–S1G).

### miR-690 treatment of NASH mice

Since miR-690 treatment had beneficial effects on fibrogenesis in liver spheroids, this prompted us to conduct *in vivo* studies in mice fed a WD, including high sucrose and cholesterol, designed to produce a NASH phenotype (NASH WD). Figure 1C shows that mice were fed the NASH WD for 16 weeks followed by treatment with nanoparticles containing the miR-690 mimic or a scrambled miRNA (Con) (5 nmol/mouse 2×/week). After 4 weeks of treatment, glucose tolerance tests (GTTs) and insulin tolerance tests (ITTs) were performed (Figures S1H and S1I), and the results show improvements in both glucose and insulin tolerance, indicative of a greater state of insulin sensitivity. Following 8 weeks of treatment, there were no significant changes in body weight or adipose tissue weight between miR-690-treated and WD control mice (Figures S1J and S1K). In contrast, liver weight was reduced in treated mice compared with WD controls (Figure S1K). In addition, miR-690-treated NASH mice showed lower levels of AST and ALT in plasma than in NASH control mice (Figure S1L). We measured whole-liver miR-690 content and found a marked (75%) decrease in miR-690 expression in NASH WD liver compared with age-matched normal chow diet (NCD) controls (Figure 1D). Following treatment, miR-690 levels increased in the mice given the miR-690 containing nanoparticles (Figure 1D). Consistent with this, we also found ~60% lower miR-690 levels in human NASH livers compared with healthy control livers (Figure 1E).

### miR-690 treatment inhibits liver fibrosis in WD NASH mice

Since progressive liver fibrosis is the most significant clinical component of NASH (Friedman, 2013; Schuppan et al., 2018; Schwabe et al., 2020), collagen content was quantitated in liver sections from control and miR-690-treated mice by evaluating Sirius Red staining. As shown in Figure 1F, there was an ~65% decrease in collagen staining in the miR-690-treated mice. With the usual immunohistochemistry method, some of the Sirius Red quantitated by microscopic analysis represents a degree of background staining. To mitigate this, we also utilized a low background Sirius Red formulation, as seen in Figure S1M. When background staining was reduced with this approach, miR-690 mimic treatment led to a greater quantitative effect with an 82% reduction, indicating negligible fibrosis in the treated NASH WD-fed mice. Consistent with the lower collagen staining, fibrogenic gene expression was reduced in livers from the miR-690-treated compared with control NASH WD mice (Figure 1G).

Since activated HSCs are the major cell type leading to collagen deposition in NASH, we assessed whether miR-690 could directly inhibit the fibrogenic program in HSCs. As seen in Figures 1H–1J, miR-690 treatment inhibited fibrogenic gene expression in both mouse and human cultured HSCs.

### miR-690 treatment reduces steatosis in WD NASH mice

H&E staining of liver sections demonstrated substantial lipid accumulation in NASH WD mice, whereas 8 weeks of miR-690 treatment led to reduced lipid droplet size and reduced overall lipid content as depicted on H&E staining in Figures 2A and S2A. In addition, biochemically measured hepatic triglyceride (Tg) content was ~40% less in the miR-690-treated mice (Figure 2B). Plasma levels of Tgs and free fatty acids were also reduced in the miR-690-treated mice (Figures S2B and S2C). As seen in Figure 2C, mRNA expression of several lipogenesis-associated genes was less in the miR-690-treated mice.

Please cite this article in press as: Gao et al., MiR-690 treatment causes decreased fibrosis and steatosis and restores specific Kupffer cell functions in NASH, Cell Metabolism (2022), https://doi.org/10.1016/j.cmet.2022.05.008



CellPress

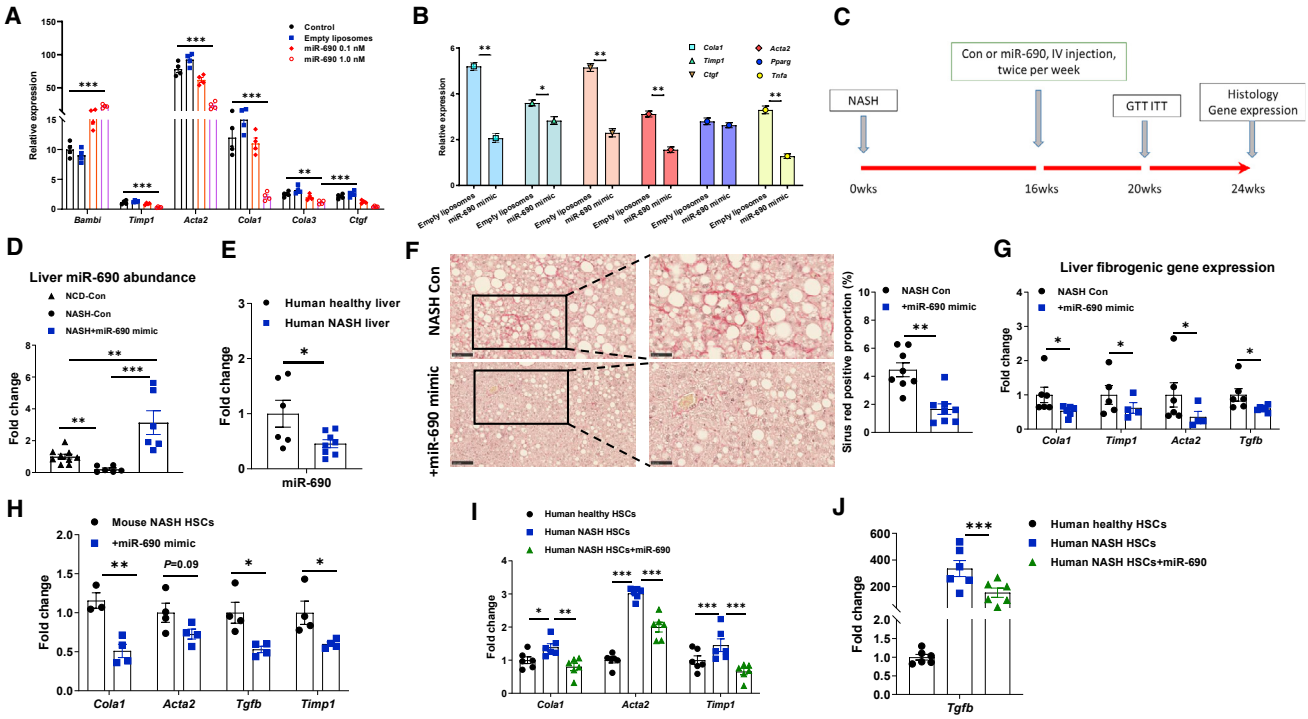


**Figure 1. miR-690 treatment inhibits fibrosis in liver spheroids or *in vivo* in WD NASH mice**

(A) Expression of fibrogenic genes in mouse liver spheroids treated with the miR-690 mimic.

(B) Effects of miR-690 mimic (1 nM) on fibrogenic or proinflammatory activation of human liver spheroids in the presence of a mixture of fatty acids (FAs), fructose, and lipopolysaccharide (LPS). n = 4 per group.

(C) Flow chart of Western diet (WD) mice injected with a scrambled RNA mimic or the miR-690 mimic. 16-week WD WT mice were intravenously injected with nanoparticles encapsulating either scrambled RNA mimic or miR-690 mimic (5 nmol/mouse, 2× per week). After 4 weeks of treatment, glucose and insulin tolerance tests (GTTs and ITTs) were performed. After 8 weeks of treatment, livers and other tissues were collected from these mice.

(D) Liver miR-690 abundance in NCD, NASH controls injected with the scrambled RNA mimic (NASH Con), and miR-690-injected NASH mice (+miR-690 mimic).

(E) miR-690 expression in human livers.

(F) Sirius Red staining of liver sections of NASH control and miR-690-injected NASH mice. Representative images of n = 8 mice per group.

(G) Liver fibrogenic gene expression in NASH control and miR-690-injected NASH mice.

(H) Fibrogenic gene expression in NASH mouse HSCs treated with the miR-690 mimic for 24 h.

(I) Fibrogenic gene expression in healthy human HSCs and NASH human HSCs treated with the miR-690 mimic for 24 h.

(J) mRNA levels of *Tgfb* in healthy human HSCs and NASH human HSCs treated with the miR-690 mimic for 24 h.

Data are presented as mean ± SEM. *p < 0.05, **p < 0.01, ***p < 0.001, Student's t test (A, B, and E–H) or one-way ANOVA (D, I, and J).

See also Figure S1.

Additionally, in isolated hepatocytes from NASH WD mice and primary human hepatocytes prepared from the livers of patients with NASH, *in vitro* treatment with miR-690 directly led to decreased lipogenic gene expression (Figures 2D and 2E) and reduced hepatocyte Tg content (Figure S2D). Thus, these studies show that miR-690 directly inhibits lipogenesis in both mouse and human hepatocytes, and this likely accounts for most of the decrease in lipid content induced by *in vivo* treatment of NASH WD mice with miR-690.

## miR-690 inhibits inflammation *in vitro* and *in vivo* in WD NASH mice

Hepatic inflammation is a key component of NASH (Inzaugarat et al., 2016; Siebler et al., 2008; Tilg and Moschen, 2010; Yu et al., 2019). As displayed in Figure 3A, when liver spheroids cultured for 14 days with FA, fructose, and LPS cocktail were treated with miR-690, cytokine gene expression, as exemplified by *Tnfa* and *Tgfb*, was markedly reduced. As expected, spheroid F4/80 expression, a marker of macrophage content, is unchanged with miR-690 treatment, since the number of seeded macrophages was constant in the different spheroid preparations. This also means that the reduced inflammatory gene expression is due to inhibition of the inflammatory program within these immune cells.

These anti-inflammatory reprogramming effects were striking when liver sections of NCD, NASH WD controls, and miR-690-treated NASH WD mice were compared by immunohistochemistry. Clec4f is a gene uniquely expressed in mouse KCs (Sakai et al., 2019; Scott et al., 2018). However, during the development of NASH, the original resident yolk sac-derived KCs undergo apoptosis and are replaced by blood monocyte-derived macrophages that enter the sinusoidal niche occupied by the previous resident KCs where they repolarize to become KC-like cells (Tran et al., 2020). The *clec4f* gene is highly specific for KCs, and immunostaining (Figure 3B) showed that KCs expressing substantial levels of Clec4f are abundant in NCD livers. Clec4f staining is

Please cite this article in press as: Gao et al., MiR-690 treatment causes decreased fibrosis and steatosis and restores specific Kupffer cell functions in NASH, Cell Metabolism (2022), https://doi.org/10.1016/j.cmet.2022.05.008



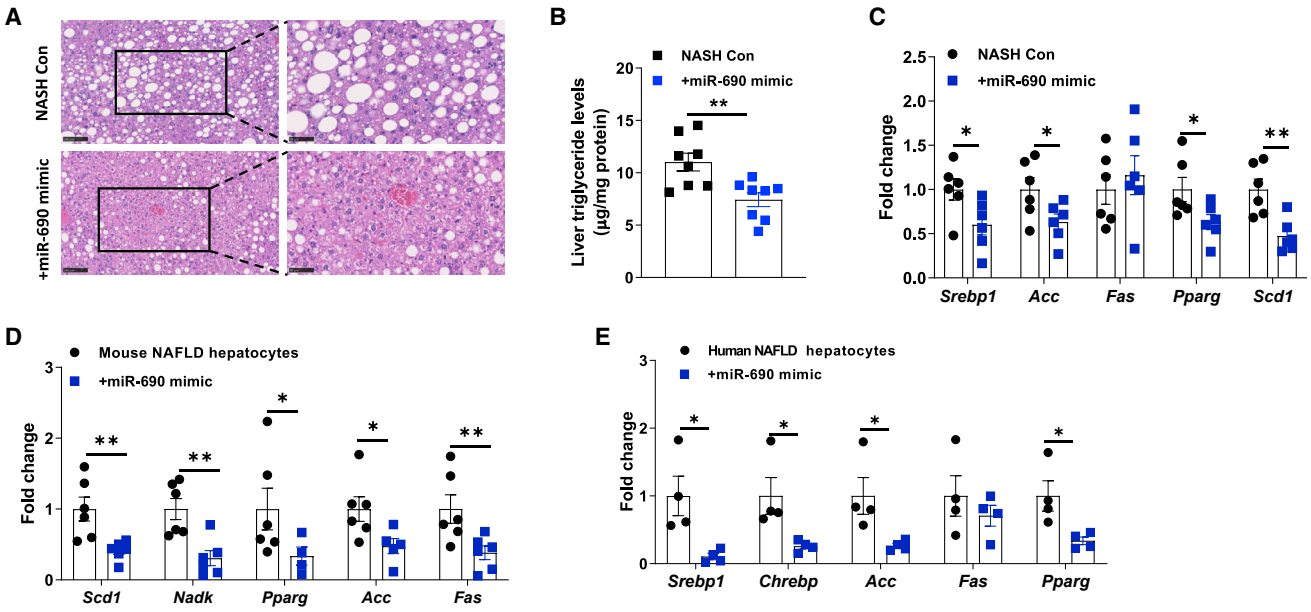


**Figure 2. miR-690 treatment reduces liver steatosis**

(A) H&E staining of liver sections of NASH Con and miR-690-treated NASH mice.

(B) Liver triglyceride (Tg) levels of NASH Con and miR-690-treated NASH mice.

(C) Lipogenesis gene expression in livers of NASH Con and miR-690-treated NASH mice.

(D) Lipogenesis gene expression in NAFLD mouse hepatocytes after 24 h treatment with the miR-690 mimic.

(E) Lipogenesis gene expression in NAFLD human hepatocytes after 24 h treatment with the miR-690 mimic.

Data are presented as mean ± SEM. *$p < 0.05$, **$p < 0.01$, ***$p < 0.001$, Student's t test.

See also Figure S2.

markedly reduced in the NASH WD mice. Most likely, this reflects that the KC-like cells express Clec4f, but at substantially reduced levels (Seidman et al., 2020; Tran et al., 2020). Importantly, upon miR-690 treatment, the liver Clec4f+ cell population was now comparable with NCD (Figures 3B and 3C).

In NCD mice, the F4/80+ cells are mostly KCs (Figure 3B), as the recruited hepatic macrophage (RHM) content of NCD liver is small. In NASH WD mice, there are greater numbers of F4/80 staining cells (Figure 3B), since monocytes are actively recruited into the liver where they differentiate into macrophages (RHMs). Based on the comparison of F4/80 staining between NCD and NASH WD mice, ~50% of the F4/80+ cells in the NASH WD mice are RHMs, whereas the remaining F4/80+ cells are KCs or KC-like cells (Figure 3B). miR-690 treatment causes a marked reduction in the number of F4/80+ liver macrophages, indicating decreased accumulation of RHMs in these mice (Figures 3B and 3C). In support of this, expression of inflammatory genes such as *Tnfa*, *Il6*, and the major liver chemokine *Ccl2* (Kazankov et al., 2019; Schuster et al., 2018) was reduced in the miR-690 treated mice compared with NASH WD controls (Figure 3D). To determine whether the effects of miR-690 on KCs were direct, we sorted KCs from the NASH WD mice and treated these cells *in vitro* with miR-690. The treatment directly reduced inflammatory gene expression, indicating direct anti-inflammatory effects of miR-690 in these cells (Figure 3E).

Cluster of differentiation 206 (CD206) is typically expressed on M2-like but not M1-like macrophages and is a useful marker for identifying anti-inflammatory phenotypes (Choi et al., 2010; Jaynes et al., 2020; Nawaz et al., 2017). Immunofluorescence staining of liver sections demonstrated readily detectable $CD206^+$ cells in the NCD group (Figure 3F). CD206 was almost exclusively expressed on the F4/80+ cells, indicating that KCs in the chow-fed state express this anti-inflammatory marker. In NASH WD mice, CD206 staining was markedly reduced (~75%), and comparing this with the corresponding F4/80 staining, this reduction in CD206 was exhibited in both KCs (or KC-like cells) and RHMs (Figures 3F, 3G, and S3A). Importantly, miR-690 treatment restored CD206 staining to NCD levels (Figures 3F and 3G). Since RHMs were markedly reduced by miR-690 treatment, this increase in CD206 expression is largely exhibited in Clec4f+ KCs (Figures 3F and 3G). To determine whether miR-690 had direct effects on the RHM polarization state, we sorted RHMs from NASH WD livers, and after 24 h of culture, we treated them with the miR-690 mimic overnight. The results shown in Figure 3H indicate that miR-690 treatment directly decreased the expression of a variety of proinflammatory genes. Thus, miR-690 treatment *in vivo* has potent anti-inflammatory effects with respect to RHMs through two mechanisms: (1) decreased content of RHMs in the liver and (2) repolarization of these cells away from the proinflammatory state. To further confirm the direct anti-inflammatory effects of miR-690, we treated LPS-induced M1 BMDMs with the miR-690 mimic and found consistent reductions in proinflammatory gene expression (Figure S3B).

In terms of systemic anti-inflammatory effects, adipose tissue from NASH WD mice as well as high-fat diet mice contains a greater number of proinflammatory M1-like macrophages compared with M2-like cells. After 8 weeks of treatment with

Please cite this article in press as: Gao et al., MiR-690 treatment causes decreased fibrosis and steatosis and restores specific Kupffer cell functions in NASH, Cell Metabolism (2022), https://doi.org/10.1016/j.cmet.2022.05.008



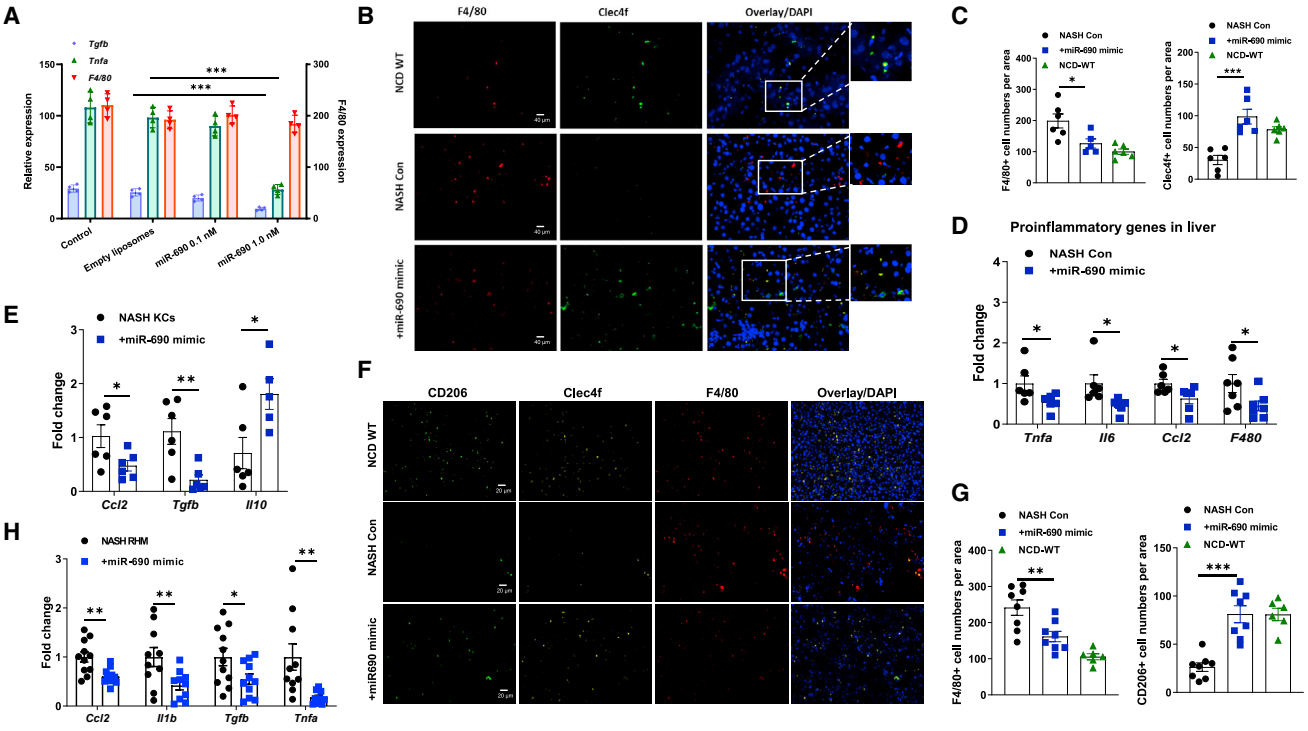


**Figure 3. miR-690 blunts inflammation in both *in vitro* and *in vivo* studies**

(A) Expression of *Tgfb*, *Tnfa*, and *F4/80* in FA, fructose, and LPS cocktail-treated liver spheroids in response to miR-690 mimic transfection.

(B and C) Immunofluorescent staining for F4/80 and Clec4f (B) and numbers of F4/80 or Clec4f-positive cells (C) in the livers of NCD WT, NASH control, and miR-690-treated NASH mice.

(D) Inflammatory gene expression in the livers of NASH Con and miR-690-treated NASH mice.

(E) The abundance of *Ccl2*, *Tgfb*, and *Il10* in mouse NASH KCs after 24 h miR-690 mimic transfection.

(F and G) Immunofluorescent staining for F4/80 and CD206 (F) and numbers of F4/80 or CD206-positive cells (G) in the livers of NCD WT, NASH Con, and miR-690-treated NASH mice.

(H) Expression of inflammatory genes in NASH recruited hepatic macrophages (RHMs) after 24 h treatment with the miR-690 mimic.

Data are presented as mean ± SEM. *p < 0.05, **p < 0.01, ***p < 0.001, Student's t test.

See also Figure S3.

miR-690, we found a substantial reduction in adipose tissue macrophage (ATM) content and a corresponding decrease in M1-like ATMs with an increase in M2 ATMs (Figure S3C). This resulted in a >50% lower ratio of M1 to M2-like ATMs.

## Effects of miR-690 treatment on KC proliferation and function

Overall, the results in Figure 3 suggest that miR-690 treatment induced functional recovery of KCs to the more homeostatic state that exists in NCD mice. Next, we determined whether miR-690 treatment could affect KC proliferation. Immunofluorescence staining of liver sections showed that treatment led to greater KC Ki67 expression *in vivo* (Figure S3D). To assess whether this effect was direct, we sorted KCs from the various mouse cohorts. After *in vitro* culture and 72 h treatment with the miR-690 mimic, we observed increased Ki67 expression in KCs (Figure S3E).

The striking effects of miR-690 treatment on Clec4f, CD206, and Ki67 staining suggest that some aspects of KC function in NASH mice are impaired and might be restored by miR-690 treatment. One of the main functions of KCs is to phagocytose senescent red blood cells (RBCs) (Terpstra and van Berkel, 2000; Willekens et al., 2005).

To assess the effects of miR-690 treatment directly on KC phagocytosis, we sorted KCs from NASH mice, cultured them overnight, and then treated them for 24 h with the miR-690 mimic. Following this, we co-cultured the KCs with senescent mouse RBCs. In Figure 4A, phagocytosed senescent RBCs are visualized as whitish dots within the individual KCs. It is evident that KCs from NCD mice take up a relatively large number of these senescent RBCs. In contrast, KCs from NASH mice phagocytose relatively few RBCs, and this defect in phagocytosis is largely restored upon treatment with miR-690 (Figure 4A). To assess this phagocytotic function in a different way, we cultured these KCs with PKH26 fluorescently labeled senescent RBCs and then analyzed the KCs by flow cytometry. Figure 4B shows the number of PKH26-labeled RBCs phagocytosed by NCD KCs in contrast to the impaired phagocytosis observed in the NASH KCs. Importantly, treatment of NASH KCs with miR-690 restored phagocytosis to normal NCD values (Figure 4B).

To explore the effects of KCs on HSC fibrogenic activation, we co-cultured NCD HSCs with NASH KCs or NCD KCs in transwell dishes. The results shown in Figure 4C indicate that co-culture with NASH KCs led to an increase in HSC fibrogenic gene expression. Co-culture with NCD KCs had small effects to

Please cite this article in press as: Gao et al., MiR-690 treatment causes decreased fibrosis and steatosis and restores specific Kupffer cell functions in NASH, Cell Metabolism (2022), https://doi.org/10.1016/j.cmet.2022.05.008



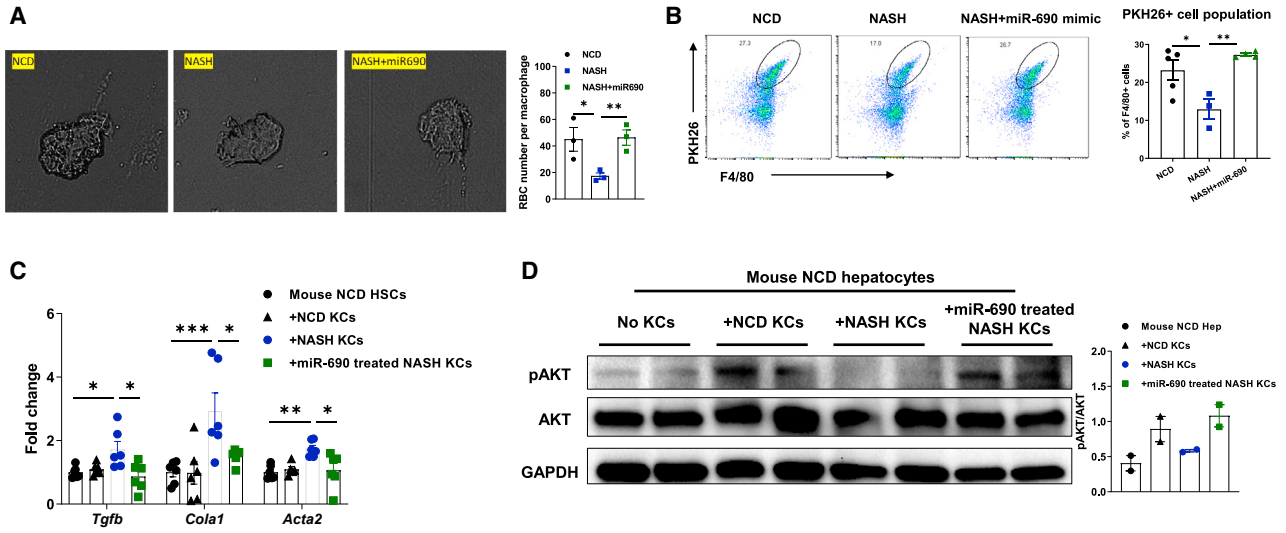


**Figure 4. Functional switch in KCs in response to NASH development**

(A) Phagocytosis of senescent RBCs by NCD WT, NASH WT, or miR-690-treated NASH WT KCs.

(B) Flow cytometry analysis of the engulfment of PKH26 labeled senescent RBCs by NCD WT, NASH WT, or miR-690-treated NASH WT KCs.

(C) Fibrogenic gene expression in NCD mouse HSCs co-cultured with NCD WT KCs, NASH WT KCs, or NASH WT KCs transfected with the miR-690 mimic.

(D) AKT phosphorylation levels in NCD mouse hepatocytes co-cultured with NCD WT KCs, NASH WT KCs, or NASH WT KCs transfected with the miR-690 mimic.

Data are presented as mean ± SEM. *p < 0.05, **p < 0.01, ***p < 0.001, one-way ANOVA (B–D).

decrease fibrogenesis. In contrast, treatment of NASH KCs with miR-690 *in vitro* completely reversed the profibrogenic effects of the NASH KCs (Figure 4C).

To determine whether KCs influence hepatocyte insulin sensitivity, NCD hepatocytes were co-cultured in transwell dishes with NCD or NASH KCs followed by measurements of phosphorylated AKT. As seen, co-culture of normal primary hepatocytes with NCD KCs leads to increased insulin-stimulated AKT phosphorylation, whereas co-culture with NASH KCs does not. Expression of miR-690 in NASH KCs restores the effect on AKT phosphorylation (Figure 4D).

## Role of miR-690 in KCs

Given that miR-690 treatment blunted the effects of NASH KCs on lipogenesis and fibrogenic activation, we measured the endogenous levels of miR-690 in NCD and NASH KCs. qPCR data in Figure 5A show that NASH KCs express less miR-690 than lean KCs. To further assess the role of miR-690 to regulate KC function, we generated KC-specific miR-690 knockout (KO) mice. These mice were produced by crossing Cas9 flox-stop-flox mice with Clec4fCre transgenic mice to establish a mouse model in which Cas9 is expressed in a KC-specific manner. These KC-specific Cas9 transgenic (Clec4fCre+Cas9+) mice received an intravenous injection of a lentivirus ($1 \times 10^8$ particles/mouse) carrying a pre-miR-690 guide RNA (gRNA-miR-690) designed to disrupt miR-690 production, as depicted in the scheme shown in Figure S4A. Figure 5B shows that this method led to ~75% depletion of KC miR-690. More importantly, depletion of miR-690 resulted in a significant reduction in the Clec4f+ KC population (Figure 5C). In addition, miR-690KO KCs displayed a functional switch from the anti-inflammatory toward a proinflammatory state (Figure 5D). *In vitro* treatment of NCD KCs with antagomiR-690 led to an attenuated anti-inflammatory phenotype and elevated expression of *Tgfb*, compared with lean WT KC controls (Figure 5E). These data indicate that the maintenance of normal endogenous miR-690 expression in NCD KCs preserves an anti-inflammatory homeostatic KC phenotype.

Our previous studies demonstrated that *Nadk*, a gene encoding NAD kinase, is a bona fide target mRNA repressed by miR-690 (Ying et al., 2021). Consistent with this, *Nadk* expression was greater in NASH KCs compared with the NCD KCs that express greater levels of miR-690 (Figure 5F). In contrast, liver NADK levels were repressed by miR-690 treatment (Figure 5G). Concomitant with the lower miR-690 abundance, the NCD miR-690KO KCs expressed a greater amount of *Nadk* than NCD WT KCs (Figure S4B). We next evaluated whether knockdown of *Nadk* could affect NASH KC function. After transfection with siRNA-*Nadk*, we found that NASH KCs exhibited improved phagocytic capacity, as evidenced by a greater number of PKH26-labeled RBCs engulfed by siRNA-*Nadk* NASH KCs than NASH KC controls (Figure S4C). Additionally, knockdown of *Nadk* blunted the effects of NASH KCs to induce fibrogenic activation in HSCs (Figure 5H). We also found that $NAD^+$ levels were lower in NASH KCs (Figure 5I). To examine whether restoring NAD affects the NASH KC phenotype, KCs isolated from NASH WT mice were treated with nicotinamide mononucleotide (NMN). After 24 h treatment, NMN-treated NASH KCs exhibited reduced expression of proinflammatory cytokines and *Tgfb* with elevated *Il10* and *Clec4f* abundance (Figure 5J).

## Intra-organ communication: KCs are the dominant source of miR-690 for other liver cells

To examine miR-690 abundance in various hepatic cells, we isolated KCs, hepatocytes, HSCs, and RHMs from lean mice. Interestingly, Figure 6A shows that NCD KCs were 2- to 4-fold more

Please cite this article in press as: Gao et al., MiR-690 treatment causes decreased fibrosis and steatosis and restores specific Kupffer cell functions in NASH, Cell Metabolism (2022), https://doi.org/10.1016/j.cmet.2022.05.008



CellPress

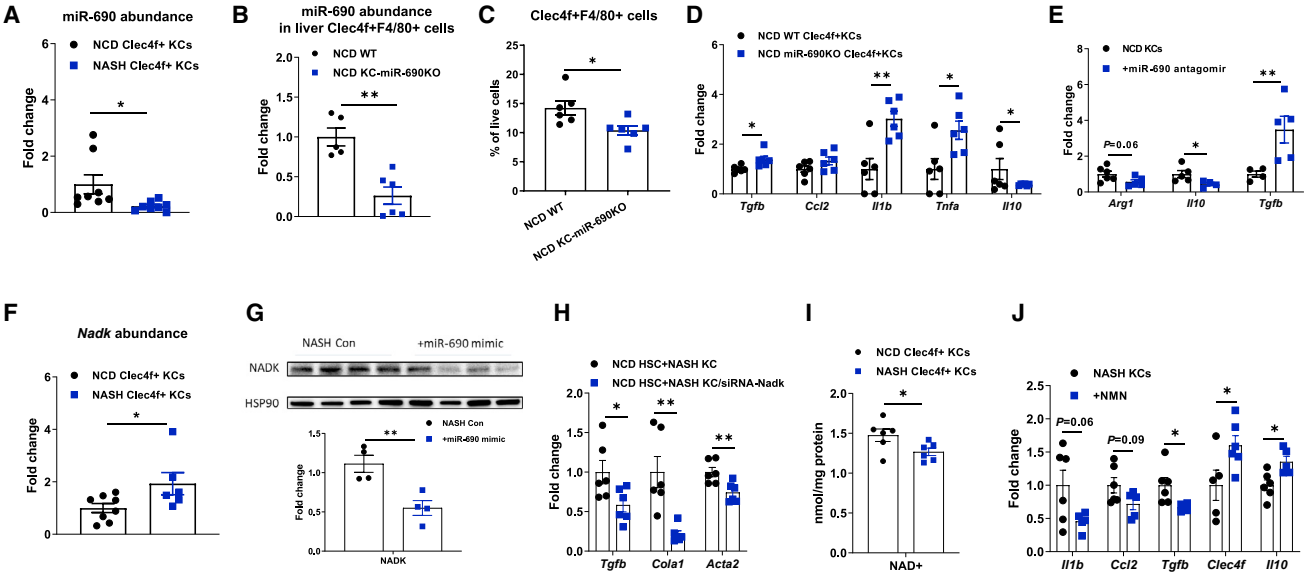


**Figure 5. miR-690 modulates KC function**

(A) miR-690 abundance in Clec4f+F4/80+ KCs of NCD WT and NASH WT mice.
(B) miR-690 abundance in Clec4f+F4/80+ KCs of NCD WT and Clec4f+ cell-specific miR-690 knockout (KC-miR-690KO) mice.
(C) Proportion of Clec4f+F4/80+ KCs in NCD WT and KC-miR-690KO mice.
(D) Inflammatory gene expression in Clec4f+F4/80+ KCs from NCD WT and KC-miR-690KO mice.
(E) Expression of *Arg1*, *Il10*, and *Tgfb* in NCD WT Clec4f+F4/80+ KCs after 24 h treatment with an miR-690 antagomir.
(F) *Nadk* expression in Clec4f+F4/80+ KCs of NCD WT and NASH WT mice.
(G) NADK abundance in the livers of NASH WT mice after 8 weeks of miR-690 treatment.
(H) Fibrogenic gene expression in NCD WT HSCs after co-culture with NASH KCs or NASH WT KCs transfected with siRNA-Nadk.
(I) $NAD^+$ levels in Clec4f+F4/80+ KCs isolated from NCD WT and NASH WT mice.
(J) Inflammatory gene abundance in NASH WT KCs after 24 h treatment with nicotinamide mononucleotide (NMN).
Data are presented as mean ± SEM. *p < 0.05, **p < 0.01, ***p < 0.001, Student's t test.
See also Figure S4.

enriched in miR-690 compared with the other cell types. In addition, concomitant with a marked reduction in KC miR-690 abundance in NASH livers, both hepatocytes and HSCs from NASH mice expressed much lower levels of miR-690 compared with hepatocytes and HSCs from NCD mice (Figures 6B and 6C). To further demonstrate the contribution of KCs to miR-690 content in neighboring cells, we utilized the diphtheria toxin (DT) depletion system to delete KCs from mice expressing the DT receptor (DTR) in a KC-specific manner using in Clec4fCre+ mice. NCD Clec4fCre+DTR+ mice were injected intraperitoneally (i.p.) with DT for 2 weeks. Following depletion of KCs, we found that both hepatocytes and HSCs expressed much less miR-690 compared with WT mice (Figures 6D and 6E). Our previous studies have shown that M2-like ATMs also express high levels of endogenous miR-690 and exosomes secreted by these ATMs could enter the circulation and contribute to miR-690 levels in hepatic cells (Ying et al., 2021). To evaluate the contribution of extrahepatic macrophages to miR-690 abundance in liver cells, NCD WT mice were treated i.p. with clodronate liposomes for 2 weeks to deplete KCs and tissue macrophages. Figures 6D and 6E show that macrophage depletion led to a marked reduction in hepatocyte and HSC miR-690 abundance, comparable with the effects of KC depletion. We next directly assessed the contribution of endogenous KC miR-690 to the miR-690 levels in hepatocytes and HSCs. In NCD KC-specific miR-690KO mice, both hepatocytes and HSCs contained lower levels of miR-690 than lean WT mice (Figures 6F and 6G). These data demonstrate that KCs are the major source of miR-690, providing this miRNA to neighboring hepatocytes, RHMs, and HSCs within the liver.

Having shown that KCs are the major source of miR-690 for neighboring liver cells, we wanted to determine whether miR-690 is shuttled from KCs via exosomes. To assess this, we generated a KC-specific Rab27 KO mouse (KC-Rab27KO; Figure S5A), since it is already known that Rab27 is critical for the secretion of exosomes from cells (Ostrowski et al., 2010) and that deletion of Rab27 inhibits exosome secretion. As presented in Figures 6H and 6I, hepatocyte and HSC miR-690 abundance were substantially decreased in the NCD KC-Rab27 KO mice. These studies demonstrate that within the liver, KC-derived exosomes convey the miR-690 from KCs to hepatocytes and HSCs. Interestingly, when we performed GTTs and ITTs in the KC-Rab27 KO mice, we found decreased glucose and insulin tolerance (Figures S5B and S5C). This is consistent with the known insulin-sensitizing effects of miR-690 and shows that in the whole mouse, KCs are a source of this miRNA, which can be released in exosomes, enter the bloodstream, and have systemic effects on glucose metabolism. Body weight was unchanged in the KC-Rab27 KO mice, compared with WT (Figure S5D).

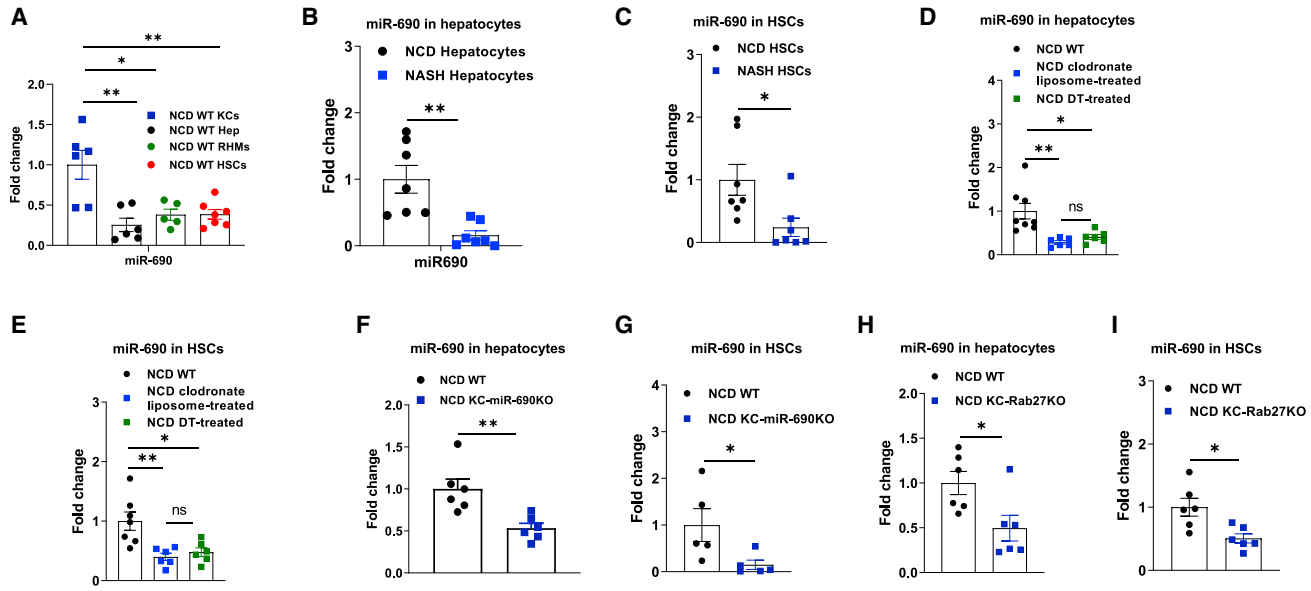


**Figure 6. KCs are the main cells secreting miR-690 into neighboring hepatic cells**

(A) miR-690 abundance in KCs, hepatocytes, RHMs, and HSCs in NCD WT livers.

(B and C) miR-690 abundance in hepatocytes (B) and HSCs (C) isolated from NCD WT and NASH WT mice.

(D and E) miR-690 abundance in hepatocytes (D) and HSCs (E) of NCD WT, clodronate liposome-treated, or diphtheria toxin (DT)-treated Clec4f+ cell-specific DTR+ mice.

(F and G) miR-690 abundance in hepatocytes (F) and HSCs (G) from NCD WT and KC-miR-690KO mice.

(H and I) miR-690 abundance in hepatocytes (H) and HSCs (I) from NCD WT and KC-Rab27KO mice.

Data are presented as mean ± SEM. *p < 0.05, **p < 0.01, ***p < 0.001, Student's t test (B–D and F–I) or one-way ANOVA (A, D, and E).

See also Figure S5.

Given that both hepatocyte and HSC miR-690 content was lower in NASH livers, we next examined whether inhibition or reduction of miR-690 levels contributes to the activation of lipogenesis and fibrogenic activation in these cell types. We addressed this question in two ways. First, after 24 h of miR-690 antagomir treatment, lean hepatocytes expressed greater levels of key genes associated with lipogenesis (Figure 7A). In addition, miR-690 antagomir treatment caused fibrogenic activation in lean HSCs, as demonstrated by upregulated expression of fibrogenic genes (Figure 7B). We also used the KC-specific miR-690KO mice to assess these. Concomitant with lower miR-690 abundance in hepatocytes and HSCs isolated from lean KC-specific miR-690KO mice, the expression of key genes associated with fibrogenic activation (Figure 7C) and lipogenesis (Figure S6A) was elevated, compared with lean WT mice. More importantly, after 16-week WD feeding, KC-specific miR-690KO mouse livers showed greater levels of lipogenic and fibrogenic gene expression compared with WT mice (Figures 7D and S6B). This was accompanied by lower levels of hepatic steatosis and fibrosis in the 16-week WD KC-specific miR-690KO mice (Figures 7E, 7F, and S6C). Since KC-specific Rab27KO leads to an ~80% reduction in hepatocyte and HSC miR-690 levels, we measured lipogenic and fibrogenic gene expression in these cells from WT and KO mice. As seen in Figures S6D and S6E, these gene programs were activated in NCD KC-specific Rab27KO mice. Together, these data suggest that maintenance of normal miR-690 abundance is necessary to keep hepatocyte lipogenesis and HSC fibrogenic activation suppressed.

## miR-690 modulates hepatocyte and HSC function through the regulation of NAD levels

Expression of the miR-690 target gene *Nadk* was upregulated in liver cells when miR-690 was inhibited with miR-690 KO or KC depletion (Figures 7G and S6E–S6H). We next assessed whether repression of *Nadk* directly affects NASH hepatocyte and HSC function. Following siRNA-*Nadk* transfection, human NAFLD hepatocytes contained less Tg than controls (Figure 7H). In addition, human NASH HSCs displayed lower fibrogenic gene expression after knockdown of *Nadk* (Figure 7I). To evaluate the importance of *Nadk* in the effects of miR-690, either human NAFLD hepatocytes or human NASH HSCs were transfected with the miR-690 mimic and/or siRNA-*Nadk*. As shown in Figures S6I and S6J, the effects of Nadk siRNA or miR-690 mimic treatment yielded comparable effects on gene expression. Furthermore, the addition of Nadk siRNA to miR-690 mimic treatment did not cause further repression of HSC fibrogenic gene levels or hepatocyte lipogenic gene expression. In addition, although treatment with the miR-690 antagomir induced hepatocyte lipogenic and HSC fibrogenic activation, co-treatment studies showed that the addition of Nadk siRNA reversed these effects (Figures S6K and S6L). Taken together, these results indicate NADK as a key target gene mediating the effects of miR-690 on NASH related phenotypes.

Consistent with the high abundance of NADK in NASH hepatocytes and HSCs, NAD levels were lower in these hepatic cells from NASH mice than in NCD mice (Figure 7J). Conversely, restoring miR-690 content led to recovery of NAD levels that

Please cite this article in press as: Gao et al., MiR-690 treatment causes decreased fibrosis and steatosis and restores specific Kupffer cell functions in NASH, Cell Metabolism (2022), https://doi.org/10.1016/j.cmet.2022.05.008



CellPress

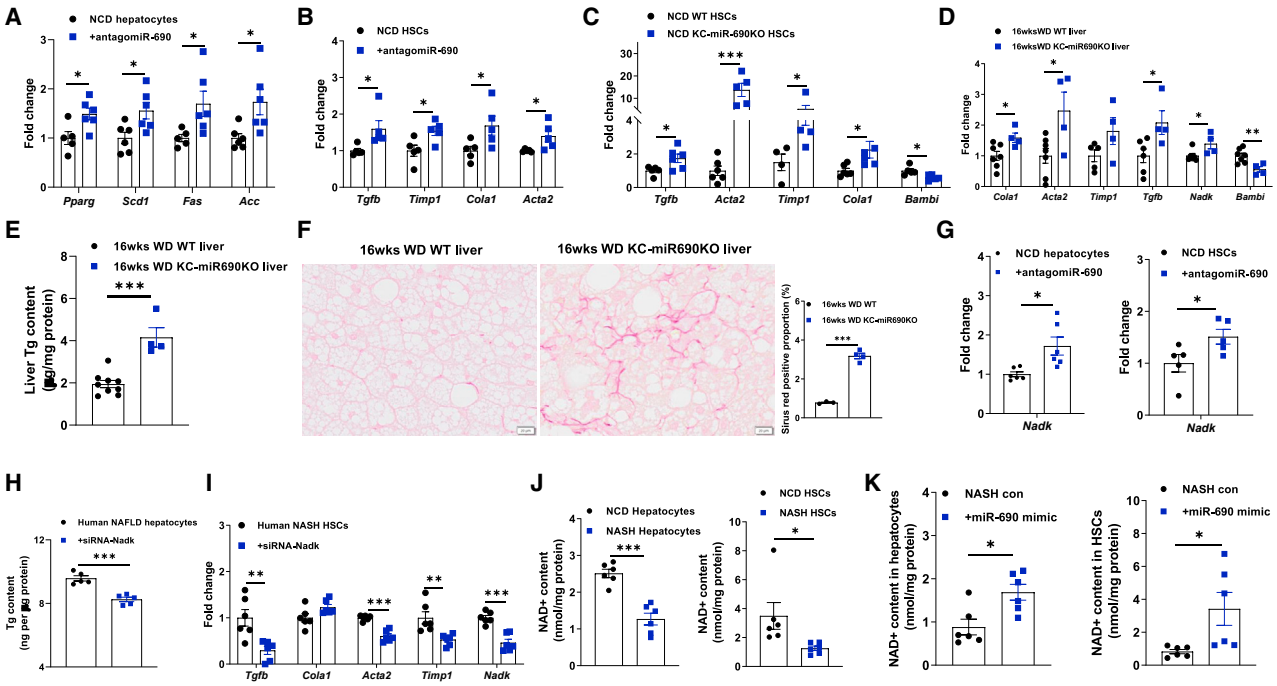


**Figure 7. miR-690 regulates hepatocyte lipogenesis and HSC fibrogenic activation through NAD abundance**

(A) Lipogenic gene abundance in NCD WT hepatocytes after 24 h treatment with an miR-690 antagomir.

(B) Expression of fibrogenic genes in NCD WT HSCs after 24 h treatment with an miR-690 antagomir.

(C) Lipogenic gene abundance in hepatocytes isolated from NCD WT and KC-miR-690KO mice.

(D) Expression of fibrogenic genes in HSCs isolated from NCD WT and KC-miR-690KO mice.

(E and F) Triglyceride levels (E) and Sirius Red staining (F) in the livers of 16-week WD WT or KC-miR-690KO mice. Representative images of n = 3–4 mice per group.

(G) *Nadk* abundance in NCD WT hepatocytes and HSCs after 24 h treatment with an miR-690 antagomir.

(H) Tg levels in human NAFLD hepatocytes treated with siRNA-Nadk.

(I) Fibrogenic gene expression in human NASH HSCs transfected with siRNA-Nadk.

(J) $NAD^+$ levels in hepatocytes and HSCs isolated from NCD WT and NASH WT mice.

(K) $NAD^+$ abundance in hepatocytes and HSCs isolated from NASH mice after 8 weeks of miR-690 treatment.

Data are presented as mean ± SEM. *p < 0.05, **p < 0.01, ***p < 0.001, Student's t test.

See also Figure S6.

were now comparable with WT NCD hepatocytes and HSCs (Figure 7K). We next assessed whether restoration of NAD content could repress NASH-associated lipogenesis and fibrosis. After treatment with the NAD precursor NMN, the expression of lipogenic genes was downregulated in NASH hepatocytes (Figure S6M). In addition, NMN treatment led to repression of fibrogenic activation in mouse and human NASH HSCs, whereas *Bambi* expression increased (Figures S6N and S6O). We also found that addition of NMN blunted the effects of the miR-690 antagomir on hepatocyte lipogenic gene and HSC fibrogenic gene expression (Figures S6K and S6L). These results are consistent with the view that the miR-690-Nadk axis exerts regulatory control of lipogenic and fibrogenic activation by modulating cellular NAD levels.

Using a bioinformatics approach, we identified "theoretical" metabolic pathway targets of miR-690 by seed sequence matching to complementary sequences in the 3′ untranslated regions of genes. The scoring for these targets is determined by how perfectly the nucleotide matching is, and we have measured the effect of miR-690 treatment to repress expression of the highest scoring "theoretical" targets in HSCs. As seen in Figure S6P, other candidate target genes of miR-690 were not affected by miR-690 treatment. Furthermore, the experiments showing that NADK knockdown is not additive to the effects of miR-690 treatment and that siRNA-Nadk reverses the effects of miR-690 antagomir treatment, all support the conclusion that NADK is a key target of miR-690. Although we cannot exclude the possibility that there are other miR-690 targets besides NADK, the data presented argue that NADK is the dominant or maybe only target of miR-690 with specific relationship to the various phenotypes and biologic effects measured in these studies.

## DISCUSSION

This study evaluated the role of the insulin-sensitizing, anti-inflammatory exosomal miR-690 on various aspects of NASH pathophysiology. Using a dietary WD NASH model, we found that treatment with an miR-690 mimic had a remarkable effect to reduce the major pathologic finding of NASH, i.e., fibrosis. This effect was quite robust, approaching normal levels in the miR-690 mimic treated mice. Consistent with this, direct

miR-690 treatment *in vitro* of either mouse or human HSCs suppressed the fibrogenic program. Steatosis was also reduced in the treated mice and could be explained by the *in vitro* effect of miR-690 to inhibit *de novo* lipogenesis (DNL) in hepatocytes.

Our studies also revealed new insights into an underappreciated role of KCs in the etiology of NASH pathogenesis. Clec4f is a highly specific marker for KCs (Sakai et al., 2019; Seidman et al., 2020), and Clec4f immunohistochemical staining was markedly reduced in NASH compared with control livers. Treatment with miR-690 increased the levels of Clec4f staining back to NCD levels. We also found that NASH KCs have a markedly reduced ability to phagocytose RBCs. NASH KCs also stimulate HSC fibrogenesis and hepatocyte DNL through secreted factors. Treatment with miR-690 reverses these effects by normalizing phagocytosis and blocking the action of KCs to induce fibrogenesis and DNL *in vitro*. In a surprising finding, we demonstrated that KCs are the dominant cell type producing miR-690 within the liver and that endogenous KC miR-690 can be shuttled through exosomes into neighboring hepatocytes and HSCs. In this way, KCs become the main supplier of miR-690 within the liver. KC miR-690 levels are markedly depressed in NASH, accounting for the decreased miR-690 levels in NASH hepatocytes and HSCs. This same reduction in miR-690 levels was also found in human NASH livers compared with healthy controls. Upon treatment of NASH mice with miR-690, levels of this miRNA rise substantially in all 3 cell types. Finally, we show that the predominant mRNA target of miR-690 is NADK and find that the corresponding increase in $NAD^+$ levels can reproduce the effects of miR-690.

As reported in previous studies, embryonic yolk sac-derived resident KCs exhibit high expression of Clec4f as a specific KC marker gene (Parthasarathy and Malhi, 2021; Sakai et al., 2019; Seidman et al., 2020). During the process of NASH development, these embryonic resident KCs undergo gradual apoptosis such that by 6 months of the WD NASH diet, ~60% of these cells are gone (Seidman et al., 2020). During the process of NASH development, monocyte-derived cells are rapidly recruited into the liver to become RHMs, and these cells sense the depleted sinusoidal niche left behind by the apoptotic embryonic KCs and move into the niche (Parthasarathy and Malhi, 2021; Seidman et al., 2020; Tacke, 2017; Tran et al., 2020). Single-cell RNA sequencing (RNA-seq) profiling of these cells indicated that they reprogram to become KC-like in their transcriptional readouts (Seidman et al., 2020). Although not identical, they are quite similar. However, Clec4f expression is reduced by ~70% in these KC-like cells compared with embryonic KCs. In addition, TIM4, which is another marker for healthy KCs, declines to near negligible levels in KC-like cells. Our studies show an ~60%–70% reduction in clec4f staining in NASH livers compared with NCD. This most likely represents the underexpression of Clec4f in the KC-like cells so that they are now poorly detected by the Clec4f antibody on immunostaining, although a reduction in immunostaining of some of the embryonic KCs cannot be excluded. Importantly, endogenous miR-690 levels are markedly reduced in NASH KCs and are completely restored following miR-690 mimic treatment. Interestingly, treatment also restores Clec4f expression to normal levels. We also observed higher Clec4f expression in isolated NASH KCs treated *in vitro* with the miR-690 mimic. Together, these results indicate that *in vivo* treatment with the miR-690 mimic directly increases Clec4f expression in NASH KCs. Since we also found that miR-690 expression enhances proliferation of KCs, as measured by Ki67 content, this raises the question of overall KC numbers in NCD, WD NASH, and WD NASH miR-690 mimic-treated mice. Although definitive quantitative numbers are difficult to obtain, $F4/80^{high}/Cd11b^{low}$ staining is also a characteristic of KCs. When we compared the total number of $F4/80^{high}/Cd11b^{low}$ cells with the number of Clec4f+ cells in NCD, WD NASH, and WD NASH miR-690 mimic-treated mice, we found that the number of KCs assessed by these two different methods was similar. Although the percent of KCs is ~50% lower in NASH compared with NCD, it should be noted that these are percentages of total $CD45^+$ cells, which represent total immune cells. In NCD, RHM abundance is very low and rises substantially in NASH, such that ~50% of $CD45^+$ cells are RHMs. Thus, the rise in RHMs largely accounts for the fall in KC%, and one can speculate that the total number of KCs is similar in NCD, NASH, and NASH-miR-690-treated livers. Perhaps the modest increase in KC proliferation with miR-690 treatment allows maintenance of KC numbers.

Along with hepatocytes, HSCs, and RHMs, KCs participate in the process of NASH pathogenesis (Bonnardel et al., 2019; Cai et al., 2020; Kisseleva and Brenner, 2021; Miura et al., 2012; Rosenthal et al., 2021). However, our current findings reveal an underappreciated role for KCs as an essential cell type that ultimately leads to the NASH phenotype. Thus, KCs, whether derived from resident yolk sac progenitor cells or RHMs that become KC-like, display functional defeats in the context of NASH. For example, NASH KCs exhibit a marked defect in phagocytosis, which is an important property of normal KCs. In addition, using transwell assays, we find that these NASH KCs can stimulate DNL in hepatocytes and activate the fibrogenic program in HSCs, and both of these pathways are key to development of NASH. The NASH KCs express much lower levels of miR-690 than normal KCs, and treatment of NASH mice *in vivo* or NASH KCs *in vitro* with the miR-690 mimic restores the properties of KCs such that they now exhibit the normal homeostatic functions of KCs from NCD mice.

It is of interest that "Clec4f" is a KC-specific gene that has been used to define this cell type. In NASH, KCs still express Clec4f, but at much lower levels than in normal KCs. The underexpression of Clec4f in NASH KCs most likely accounts for the decreased number of Clec4f+ cells observed in NASH livers because the level of expression of Clec4f in a proportion of NASH KCs is below the detection level by the immunostaining antibodies. Treatment with the miR-690 mimic restores Clec4f immunostaining to normal, consistent with the effect of miR-690 to promote KC function.

As further evidence that miR-690 in KCs plays an important role in NASH pathogenesis, we also conducted studies on KC-specific miR-690KO mice. On the WD NASH diet, these KO mice developed enhanced fibrosis and other features of NASH, including increased expression of fibrogenic and inflammatory genes. This provides a second NASH model, supporting the role of KC miR-690 in the etiology of this disease.

The etiology of NASH involves abnormalities in a number of liver cell types, including hepatocytes, HSCs, KCs, and RHMs. Previous depictions have placed the hepatocyte in the center

of this nexus, since it is responsible for the initial steatosis observed in NAFLD and might release toxic factors such as lipids, cytokines, or other substances that negatively impact HSCs and hepatic macrophages. The current studies suggest that KCs may play a more integral role in NASH pathogenesis than realized, since the NASH-induced deficiency of miR-690 in KCs confers the ability of these KCs to stimulate DNL in hepatocytes and activate the fibrogenic program in HSCs. Clearly, the ultimate expression of the NASH phenotype involves a collaboration between all of these cell types.

These studies show that miR-690 has direct effects on HSCs to inhibit the fibrogenic program, which is clearly a beneficial effect in the context of NASH. Fibrosis is also a feature of several other diseases, such as pulmonary and renal diseases. Whether this miRNA has any anti-fibrotic actions in these conditions is currently unknown.

We cannot rule out that there may be other miRNAs besides miR-690 within M2 BMDM exosomes that contribute to these beneficial effects, but our data indicate that miR-690 is either entirely responsible or that it is certainly the dominant miRNA involved. The normal endogenous expression levels of miR-690 in NCD KCs fall dramatically during the progression to NASH. The mechanism for the downregulation of miR-690 is unknown. miR-690 was localized to intron 2 of the FGF12 gene. This suggests that regulation of miR-690 most likely reflects posttranscriptional modifications within KCs through mechanisms that remain to be clarified.

In summary, these studies show that exosomal miR-690 has a powerful role to prevent and/or treat NASH. Upon the development of NASH, miR-690 levels are markedly reduced in the liver. This is primarily due to decreased KC miR-690 levels. Endogenous miR-690 within KCs is secreted via exosomes and is the main supply mechanism providing this miRNA to neighboring hepatocytes and HSCs. miR-690 mimic treatment of NASH mice has substantial effects to inhibit many aspects of NASH pathophysiology, including fibrosis, steatosis, and inflammation by returning to normal the three critical cell types in the liver: hepatocytes, KCs, and HSCs. Thus, in addition to the systemic effects observed with *in vivo* 690 mimic treatment, miR-690 also has direct effects to inhibit fibrogenesis in mouse and human HSCs, repress DNL in hepatocytes, and reduce the inflammatory tone of macrophages. The key target of miR-690 we have identified is NADK mRNA and suppression of NADK via miR-690 leads to a rise in cellular and total liver $NAD^+$ levels. Functional studies reveal that restoring $NAD^+$ levels in NASH cells can reproduce the beneficial effects of miR-690 treatment, consistent with previous studies showing that $NAD^+$ supplementation can reduce liver fibrosis (Pham et al., 2019; Zong et al., 2021). These studies reveal new aspects of KC biology within the context of NASH and also suggest that, if translated to humans, miR-690 treatment could become a therapeutic tool.

### Limitations of study

Although it is known from previous publications that NASH KCs consist of a population of original embryonic KCs as well as KC-like cells derived from RHMs, our methods do not allow us to discriminate between these two KC populations with respect to the percentage or total number of KCs. Furthermore, we cannot determine the extent to which the various functional defects we have measured in total KCs exists in embryonic-derived KCs versus KC-like cells. In addition, although we show clear evidence that NADK is a major target of miR-690 and that replenishment of NAD in NASH can reproduce the beneficial effects of miR-690 treatment, the detailed mechanisms of how the NADK/NAD system interacts with the NASH etiology remain to be determined. This will require studies of an inducible hepatocyte-specific NADK KO mouse model. Finally, although most of the studies were conducted in mice, human cells were used in many of the *in vitro* experiments. We were also able to demonstrate that miR-690 was depleted in human NASH livers as it was in mice. However, it remains to be determined whether the beneficial effects of miR-690 observed in NASH mice can be translated to humans.

## STAR★METHODS

Detailed methods are provided in the online version of this paper and include the following:

- KEY RESOURCES TABLE
- RESOURCE AVAILABILITY
  - Lead contact
  - Materials availability
  - Data and code availability
- EXPERIMENTAL MODEL AND SUBJECT DETAILS
  - Mice
  - Study approval
  - Human specimens
- METHOD DETAILS
  - Isolation of primary hepatocytes
  - Hepatic stellate cell (HSC) isolation
  - Co-culture assay
  - Hepatic Spheroid culture
  - Triglyceride detection
  - Glucose tolerance (GTT) and insulin tolerance tests (ITT)
  - siRNA transfection
  - miR-690 mimic transfection or *in vivo* treatment
  - Immuno-fluorescence staining
  - Quantitative Reverse Transcriptase-polymerase Chain Reaction (RT-PCR) Analysis
  - Western blot analysis
- QUANTIFICATION AND STATISTICAL ANALYSIS

## SUPPLEMENTAL INFORMATION

Supplemental information can be found online at https://doi.org/10.1016/j.cmet.2022.05.008.

## ACKNOWLEDGMENTS

We thank the UCSD microscopy core for microscopic analysis, the UCSD Moore Cancer Center histology core for H&E and Sirius Red staining, and the Vector Development Core Laboratory for lentivirus preparation. We thank Jachelle Pimentel for excellent administration assistance and Alessandro Pocai and Pejman Soroosh (Janssen Pharmaceuticals) for helpful discussions. This study was funded by National Institutes of Health grants (NINDS P30 NS047101 to the UCSD microscopy core; P30 DK063491, R00DK115998, and R01DK125560 to W.Y.; R01DK101737, U01AA022614, R01DK099205, R01DK111866, R01AA028550, P50AA011999, U01AA018663, P30 DK120

515, 5U01AA029019, R01DK091183, and R01DK09920 to T.K.; P50AA011999, P42ES010337, and R44DK115242 to D.A.B.; and DK063491 and DK101395 to J.M.O.) and a grant from Janssen Pharmaceuticals to J.M.O.

## AUTHOR CONTRIBUTIONS

H.G., W.Y., and J.M.O. designed the studies, and H.G. performed most of the experiments. G.B. performed liver spheroid assays. Z.J., D.Z., and K.C.E.R. assisted with tissue collection, cell culture, qPCR analysis, and western blot analysis. H.J. and S.P. prepared nanoparticles/microRNA mimic. X.L., H.Z., T.K., and D.A.B. contributed the human liver samples. W.Y. and J.M.O. supervised the project. H.G., W.Y., and J.M.O. analyzed and interpreted the data and co-wrote the manuscript.

## DECLARATION OF INTERESTS

W.Y. and J.M.O. are co-investigators on a provisional patent covering the use of miR-690 as an insulin sensitizer.

Received: January 12, 2022
Revised: April 7, 2022
Accepted: May 20, 2022
Published: June 13, 2022

## REFERENCES

Alexander, M., Hu, R., Runtsch, M.C., Kagele, D.A., Mosbruger, T.L., Tolmachova, T., Seabra, M.C., Round, J.L., Ward, D.M., and O'Connell, R.M. (2015). Exosome-delivered microRNAs modulate the inflammatory response to endotoxin. Nat. Commun. *6*, 7321.

Anstee, Q.M., Targher, G., and Day, C.P. (2013). Progression of NAFLD to diabetes mellitus, cardiovascular disease or cirrhosis. Nat. Rev. Gastroenterol. Hepatol. *10*, 330–344.

Bonnardel, J., T'Jonck, W., Gaublomme, D., Browaeys, R., Scott, C.L., Martens, L., Vanneste, B., De Prijck, S., Nedospasov, S.A., Kremer, A., et al. (2019). Stellate cells, hepatocytes, and endothelial cells imprint the Kupffer cell identity on monocytes colonizing the liver macrophage niche. Immunity *51*, 638–654.e9.

Broutier, L., Andersson-Rolf, A., Hindley, C.J., Boj, S.F., Clevers, H., Koo, B.-K., and Huch, M. (2016). Culture and establishment of self-renewing human and mouse adult liver and pancreas 3D organoids and their genetic manipulation. Nat. Protoc. *11*, 1724–1743.

Cai, B., Dongiovanni, P., Corey, K.E., Wang, X., Shmarakov, I.O., Zheng, Z., Kasikara, C., Davra, V., Meroni, M., Chung, R.T., et al. (2020). Macrophage MerTK promotes liver fibrosis in nonalcoholic steatohepatitis. Cell Metab. *31*, 406–421.e7.

Choi, K.M., Kashyap, P.C., Dutta, N., Stoltz, G.J., Ordog, T., Shea Donohue, T., Bauer, A.J., Linden, D.R., Szurszewski, J.H., Gibbons, S.J., et al. (2010). CD206-positive M2 macrophages that express heme Oxygenase-1 protect against diabetic gastroparesis in mice. Gastroenterology *138*, 2399–2409.e1.

Elbadawy, M., Yamanaka, M., Goto, Y., Hayashi, K., Tsunedomi, R., Hazama, S., Nagano, H., Yoshida, T., Shibutani, M., Ichikawa, R., et al. (2020). Efficacy of primary liver organoid culture from different stages of non-alcoholic steatohepatitis (NASH) mouse model. Biomaterials *237*, 119823.

Friedman, S.L. (2013). Liver fibrosis in 2012: convergent pathways that cause hepatic fibrosis in NASH. Nat. Rev. Gastroenterol. Hepatol. *10*, 71–72.

Friedman, S.L., Neuschwander-Tetri, B.A., Rinella, M., and Sanyal, A.J. (2018). Mechanisms of NAFLD development and therapeutic strategies. Nat. Med. *24*, 908–922.

Inzaugarat, M.E., Wree, A., and Feldstein, A.E. (2016). Hepatocyte mitochondrial DNA released in microparticles and toll-like receptor 9 activation: a link between lipotoxicity and inflammation during nonalcoholic steatohepatitis. Hepatology *64*, 669–671.

Isaac, R., Reis, F.C.G., Ying, W., and Olefsky, J.M. (2021). Exosomes as mediators of intercellular crosstalk in metabolism. Cell Metab. *33*, 1744–1762.

Jaynes, J.M., Sable, R., Ronzetti, M., Bautista, W., Knotts, Z., Abisoye-Ogunniyan, A., Li, D., Calvo, R., Dashnyam, M., Singh, A., et al. (2020). Mannose receptor (CD206) activation in tumor-associated macrophages enhances adaptive and innate antitumor immune responses. Sci. Transl. Med. *12*, eaax6337.

Kazankov, K., Jørgensen, S.M.D., Thomsen, K.L., Møller, H.J., Vilstrup, H., George, J., Schuppan, D., and Grønbæk, H. (2019). The role of macrophages in nonalcoholic fatty liver disease and nonalcoholic steatohepatitis. Nat. Rev. Gastroenterol. Hepatol. *16*, 145–159.

Kisseleva, T., and Brenner, D. (2021). Molecular and cellular mechanisms of liver fibrosis and its regression. Nat. Rev. Gastroenterol. Hepatol. *18*, 151–166.

Lee, Y.A., and Friedman, S.L. (2022). Inflammatory and fibrotic mechanisms in NAFLD—implications for new treatment strategies. J. Intern. Med. *291*, 11–31.

Li, P., Liu, S., Lu, M., Bandyopadhyay, G., Oh, D., Imamura, T., Johnson, A.M.F., Sears, D., Shen, Z., Cui, B., et al. (2016). Hematopoietic-derived galectin-3 causes cellular and systemic insulin resistance. Cell *167*, 973–984.e12.

McCarron, S., Bathon, B., Conlon, D.M., Abbey, D., Rader, D.J., Gawronski, K., Brown, C.D., Olthoff, K.M., Shaked, A., and Raabe, T.D. (2021). Functional characterization of organoids derived from irreversibly damaged liver of patients with NASH. Hepatology *74*, 1825–1844.

Miura, K., Yang, L., van Rooijen, N., Ohnishi, H., and Seki, E. (2012). Hepatic recruitment of macrophages promotes nonalcoholic steatohepatitis through CCR2. Am. J. Physiol. Gastrointest. Liver Physiol. *302*, G1310–G1321.

Nawaz, A., Aminuddin, A., Kado, T., Takikawa, A., Yamamoto, S., Tsuneyama, K., Igarashi, Y., Ikutani, M., Nishida, Y., Nagai, Y., et al. (2017). CD206+ M2-like macrophages regulate systemic glucose metabolism by inhibiting proliferation of adipocyte progenitors. Nat. Commun. *8*, 286.

Noureddin, M., Vipani, A., Bresee, C., Todo, T., Kim, I.K., Alkhouri, N., Setiawan, V.W., Tran, T., Ayoub, W.S., Lu, S.C., et al. (2018). NASH leading cause of liver transplant in women: updated analysis of indications for liver transplant and ethnic and gender variances. Am. J. Gastroenterol. *113*, 1649–1659.

Ostrowski, M., Carmo, N.B., Krumeich, S., Fanget, I., Raposo, G., Savina, A., Moita, C.F., Schauer, K., Hume, A.N., Freitas, R.P., et al. (2010). Rab27a and Rab27b control different steps of the exosome secretion pathway. Nat. Cell Biol. *12*, 19–30.

Parthasarathy, G., and Malhi, H. (2021). Macrophage heterogeneity in NASH: more than just nomenclature. Hepatology *74*, 515–518.

Pham, T.X., Bae, M., Kim, M.B., Lee, Y., Hu, S., Kang, H., Park, Y.K., and Lee, J.Y. (2019). Nicotinamide riboside, an $NAD^+$ precursor, attenuates the development of liver fibrosis in a diet-induced mouse model of liver fibrosis. Biochim. Biophys. Acta Mol. Basis Dis. *1865*, 2451–2463.

Prior, N., Inacio, P., and Huch, M. (2019). Liver organoids: from basic research to therapeutic applications. Gut *68*, 2228–2237.

Rosenthal, S.B., Liu, X., Ganguly, S., Dhar, D., Pasillas, M.P., Ricciardelli, E., Li, R.Z., Troutman, T.D., Kisseleva, T., Glass, C.K., et al. (2021). Heterogeneity of HSCs in a mouse model of NASH. Hepatology *74*, 667–685.

Sakai, M., Troutman, T.D., Seidman, J.S., Ouyang, Z., Spann, N.J., Abe, Y., Ego, K.M., Bruni, C.M., Deng, Z., and Schlachetzki, J.C.M. (2019). Liver-derived signals sequentially reprogram myeloid enhancers to initiate and maintain Kupffer cell identity. Immunity *51*, 655–670.e8.

Schuppan, D., Surabattula, R., and Wang, X.Y. (2018). Determinants of fibrosis progression and regression in NASH. J. Hepatol. *68*, 238–250.

Schuster, S., Cabrera, D., Arrese, M., and Feldstein, A.E. (2018). Triggering and resolution of inflammation in NASH. Nat. Rev. Gastroenterol. Hepatol. *15*, 349–364.

Schwabe, R.F., Tabas, I., and Pajvani, U.B. (2020). Mechanisms of fibrosis development in nonalcoholic steatohepatitis. Gastroenterology *158*, 1913–1928.

Scott, C.L., T'Jonck, W., Martens, L., Todorov, H., Sichien, D., Soen, B., Bonnardel, J., De Prijck, S., Vandamme, N., and Cannoodt, R. (2018). The transcription factor ZEB2 is required to maintain the tissue-specific identities of macrophages. Immunity *49*, 312–325.e5.

Seidman, J.S., Troutman, T.D., Sakai, M., Gola, A., Spann, N.J., Bennett, H., Bruni, C.M., Ouyang, Z., Li, R.Z., Sun, X., et al. (2020). Niche-specific reprogramming of epigenetic landscapes drives myeloid cell diversity in nonalcoholic steatohepatitis. Immunity *52*, 1057–1074.e7.

Sheka, A.C., Adeyi, O., Thompson, J., Hameed, B., Crawford, P.A., and Ikramuddin, S. (2020). Nonalcoholic steatohepatitis: a review. JAMA *323*, 1175–1183.

Siebler, J., Galle, P.R., and Weber, M.M. (2008). The gut-liver-axis: endotoxemia, inflammation, insulin resistance and NASH. J. Hepatol. *48*, 1032–1034.

Tabas, I., and Glass, C.K. (2013). Anti-inflammatory therapy in chronic disease: challenges and opportunities. Science *339*, 166–172.

Tacke, F. (2017). Targeting hepatic macrophages to treat liver diseases. J. Hepatol. *66*, 1300–1312.

Terpstra, V., and van Berkel, T.J.C. (2000). Scavenger receptors on liver Kupffer cells mediate the in vivo uptake of oxidatively damaged red blood cells in mice. Blood *95*, 2157–2163.

Tilg, H., and Moschen, A.R. (2010). Evolution of inflammation in nonalcoholic fatty liver disease: the multiple parallel hits hypothesis. Hepatology *52*, 1836–1846.

Tkach, M., and Théry, C. (2016). Communication by extracellular vesicles: where we are and where we need to go. Cell *164*, 1226–1232.

Tran, S., Baba, I., Poupel, L., Dussaud, S., Moreau, M., Gélineau, A., Marcelin, G., Magréau-Davy, E., Ouhachi, M., and Lesnik, P. (2020). Impaired Kupffer cell self-renewal alters the liver response to lipid overload during non-alcoholic steatohepatitis. Immunity *53*, 627–640.e5.

Wesolowski, S.R., Kasmi, K.C.E., Jonscher, K.R., and Friedman, J.E. (2017). Developmental origins of NAFLD: a womb with a clue. Nat. Rev. Gastroenterol. Hepatol. *14*, 81–96.

Willekens, F.L.A., Werre, J.M., Kruijt, J.K., Roerdinkholder-Stoelwinder, B., Groenen-Döpp, Y.A.M., van den Bos, A.G., Bosman, G.J., and van Berkel, T.J.C. (2005). Liver Kupffer cells rapidly remove red blood cell-derived vesicles from the circulation by scavenger receptors. Blood *105*, 2141–2145.

Ying, W., Riopel, M., Bandyopadhyay, G., Dong, Y., Birmingham, A., Seo, J.B., Ofrecio, J.M., Wollam, J., Hernandez-Carretero, A., Fu, W., et al. (2017). Adipose tissue macrophage-derived exosomal miRNAs can modulate *in vivo* and *in vitro* insulin sensitivity. Cell *171*, 372–384.e12.

Ying, W., Gao, H., Dos Reis, F.C.G., Bandyopadhyay, G., Ofrecio, J.M., Luo, Z., Ji, Y., Jin, Z., Ly, C., and Olefsky, J.M. (2021). MiR-690, an exosomal-derived miRNA from M2-polarized macrophages, improves insulin sensitivity in obese mice. Cell Metab. *33*, 781–790.e5.

Yu, J., Shen, J., Sun, T.T., Zhang, X., and Wong, N. (2013). Obesity, insulin resistance, NASH and hepatocellular carcinoma. Semin. Cancer Biol. *23*, 483–491.

Yu, Y., Liu, Y., An, W., Song, J., Zhang, Y., and Zhao, X. (2019). STING-mediated inflammation in Kupffer cells contributes to progression of nonalcoholic steatohepatitis. J. Clin. Invest. *129*, 546–555.

Zhu, C.Y., Tabas, I., Schwabe, R.F., and Pajvani, U.B. (2021). Maladaptive regeneration—the reawakening of developmental pathways in NASH and fibrosis. Nat. Rev. Gastroenterol. Hepatol. *18*, 131–142.

Zong, Z., Liu, J., Wang, N., Yang, C., Wang, Q., Zhang, W., Chen, Y., Liu, X., and Deng, H. (2021). Nicotinamide mononucleotide inhibits hepatic stellate cell activation to prevent liver fibrosis via promoting PGE2 degradation. Free Radic. Biol. Med. *162*, 571–581.

Please cite this article in press as: Gao et al., MiR-690 treatment causes decreased fibrosis and steatosis and restores specific Kupffer cell functions in NASH, Cell Metabolism (2022), https://doi.org/10.1016/j.cmet.2022.05.008



## STAR★METHODS

### KEY RESOURCES TABLE

| REAGENT or RESOURCE | SOURCE | IDENTIFIER |
|---|---|---|
| Antibodies | | |
| Anti-HSP90 | Santa Cruz | Cat# sc-101494; RRID: AB_1124018 |
| Anti-Phospho-AKT Ser473 | Cell signaling technology | Cat# 9271S; RRID: AB_329825 |
| Anti-pan AKT | Cell signaling technology | Cat# 4691S; RRID: AB_915783 |
| Anti-Clec4f-APC | BioLegend | Cat# 156803; RRID: AB_2814081 |
| Anti-F4/80-PE | BioLegend | Cat# 123109; RRID: AB_893498 |
| Anti-F4/80-PE Cy7 | BioLegend | Cat# 123113; RRID: AB_893490 |
| Anti-Cd45-APC Cy7 | BioLegend | Cat# 103115; RRID: AB_312980 |
| Anti-Cd11b-FITC | BioLegend | Cat# 101205; RRID: AB_312788 |
| Anti-CD206 | BioLegend | Cat# 141706; RRID: AB_10896421 |
| Anti-Ki67 | BioLegend | Cat# 652405; RRID: AB_2561929 |
| Anti-NADK | Cell signaling technology | Cat# 55948S; RRID: AB_2799500 |
| Chemicals, peptides, and recombinant proteins | | |
| Live/Dead Fixable Aqua dead cell stain kit | ThermoFisher | Cat# L34966 |
| Novolin R regular human insulin used in ITTs | Novo-Nordisk | Cat# NDC 0169-1833-11 |
| Dextrose | Hospira | Cat# 0409-6648-02 |
| Collagenase II | Sigma-Aldrich | Cat# C2674 |
| Percoll | GE Healthcare Life Sciences | Cat# 17-0891-01 |
| TRIzol RNA isolation reagent | ThermoFisher Scientific | Cat# 15596026 |
| SuperSignal West Pico Chemiluminescent Substrate | ThermoFisher Scientific | Cat# 34077 |
| Halt Protease and Phosphatase Inhibitor Cocktail | ThermoFisher Scientific | Cat# 78440 |
| RIPA buffer (10x) | Cell Signaling Technology | Cat# 9806 |
| PKH26 | Sigma-Aldrich | Cat# PKH26GL-1KT |
| AIN76A Western Diet | TestDiet | Cat# 5342 |
| Pronase | Roche | Cat# 11459643001 |
| Collagenase D | Roche | Cat# 11088882001 |
| DNAnase I | Roche | Cat# 10104159001 |
| RBC lysis buffer | eBioscience | Cat# 00-4333-57 |
| High-capacity cDNA reverse transcription kit | ThermoFisher Scientific | Cat# 4368813 |
| iTaq SYBR Green supermix | Bio-Rad | Cat# 172-5125 |
| Lipofectamine RNAiMAX reagent | ThermoFisher Scientific | Cat# 13778-075 |
| TaqMan microRNA reverse transcription kit | ThermoFisher Scientific | Cat#4366597 |
| TaqMan universal master mix II | ThermoFisher Scientific | Cat#4440040 |
| LPS | Sigma | Cat# L2630-10MG |
| DT (Diphtheria Toxin) | Bio Academia | Cat# 01-517 |
| Mouse collagen I ELISA kit | AVIVA systems biology | Cat# OKEH00544 |
| Mouse TIMP1 ELISA kit | RayBiotech | Cat# ELM-TIMP1-1 |
| Human collagen I ELISA kit | LSBio | Cat# LS-F29615-1 |
| Human TIMP1 ELISA kit | RayBiotech | Cat# ELH-TIMP-1 |
| Human MCP1 ELISA kit | Biolegend | Cat# 438807 |
| Free fatty acid kit | Wako | Cat# TH618 |
| Triglyceride kit | Cayman | Cat# 10010303-96 |

(*Continued on next page*)

Please cite this article in press as: Gao et al., MiR-690 treatment causes decreased fibrosis and steatosis and restores specific Kupffer cell functions in NASH, Cell Metabolism (2022), https://doi.org/10.1016/j.cmet.2022.05.008





*Continued*

| REAGENT or RESOURCE | SOURCE | IDENTIFIER |
|---|---|---|
| $NAD^+$ Assay Kit | EnzyChrom | Cat# E2ND |
| Critical commercial assays | | |
| Quick-RNA microprep kit | Zymo research | Cat# R1051 |
| Deposited data | | |
| Raw data for graphs and blots | Data S1 | N/A |
| Experimental models: Organisms/strains | | |
| Mouse: WT C57BL6/J | Jackson Laboratories | JAX: 000664 |
| Mouse: *Rosa26-floxed STOP-Cas9* | Jackson Laboratories | JAX: 028551 |
| Mouse: *B6-iDTR, ROSA26iDTR* | Jackson Laboratories | JAX: 007900 |
| Mouse: *Clec4f-Cre-tdTomato* | Jackson Laboratories | JAX: 033296 |
| Oligonucleotides | | |
| siRNA-mouse NADK | Horizon Discovery | Cat# J-053672-05-0002 |
| siRNA-human NADK | Horizon Discovery | Cat# J-006318-05-0002 |
| miR-690 RT-PCR primer | ThermoFisher Scientific | Assay ID: 001677 |
| U6 snRNA RT-PCR primer | ThermoFisher Scientific | Assay ID: 001973 |
| miR-690 mimic | ThermoFisher Scientific | Cat# 4464066 |
| miRNA mimic negative control | ThermoFisher Scientific | Cat# 4464058 |
| Edit-R custom lentiviral sgRNA mir690 | Horizon Discovery | Cat# sgRNA-688383 |
| gRNA-Rab27a | Sigma | Sanger Clone ID: MM5000028879 |
| gRNA-Rab27b | Sigma | Sanger Clone ID: MM5000025441 |
| Software and algorithms | | |
| Prism | Graphpad | https://www.graphpad.com/scientific-software/prism/ |
| FlowJo | FlowJo | N/A |
| ImageJ | NIH | https://imagej.nih.gov/ij/ |

## RESOURCE AVAILABILITY

### Lead contact

Further information and requests for resources and reagents should be directly to and will be fulfilled by the lead contact, Jerrold M. Olefsky (jolefsky@health.ucsd.edu).

### Materials availability

All mouse lines in this study are available from the Jackson Laboratory.

### Data and code availability

Original data for creating all graphs in the paper are provide in Data S1.

## EXPERIMENTAL MODEL AND SUBJECT DETAILS

### Mice

C57BL/6 (B6) mice were fed an AIN76A NASH Western Diet (WD; TestDiet 5342; containing 40% fat calorie and 0.15% cholesterol) or a normal chow diet (NCD) ad libitum. To evaluate the effects of miR-690 on the development of liver steatosis and fibrosis, 16wks WD B6 WT mice were intravenously injected with nanoparticles encapsulating either a scrambled RNA mimic or the miR-690 mimic (5 nmole/mouse, 2X per week). After 4 weeks (wks) of treatment, glucose and insulin tolerance tests (GTTs and ITTs) were performed. After 8wks of treatment, livers and other tissues were collected from these mice. To generate Kupffer cell-specific Cas9 transgenic mice, Rosa26-floxed STOP-Cas9 knockin mice were bred with Clec4f-Cre mice. To generate Kupffer cell-specific miR-690 knockout, Kupffer cell-specific Cas9 transgenic mice were intravenously injected with a lentivirus carrying gRNA-pre-miR-690 ($1\times10^8$ particles per mouse). To generate Kupffer cell-specific knockout of Rab27, Kupffer cell-specific Cas9 transgenic mice were intravenously injected with a lentivirus carrying gRNA-Rab27 ($1\times10^8$ particles per mouse). Kupffer cell-specific Cas9 transgenic mice treated with lentivirus carrying empty vectors were used as controls. To deplete Kupffer cells, diphtheria toxin (DT) was intraperitoneally (200 ng/mouse, i.p.) injected into $Clec4fCre^+DTR^+$ lean mice for three days, and these mice were treated with DT

(200 ng/mouse) every two days to prevent KC recovery (KCKO). All mice used in this study were male and maintained at 22°C in a 12/12-h light/dark cycle in a specific pathogen-free facility and given free access to food and water.

### Study approval

All animal procedures were done in accordance with University of California, San Diego Research Guidelines for the Care and Use of Laboratory Animals and all animals were randomly assigned to cohorts when used.

### Human specimens

Deidentified livers declined for transplantation are used in this study, the patient consent was obtained by https://www.lifesharing.org/. This project has been reviewed by the Director of the UCSD HRPP, IRB Chair, or IRB Chair's designee and is certified as not qualifying as human subjects research according to the Code of Federal Regulations, Title 45, part 46 and UCSD Standard Operating Policies and Procedures, and therefore does not require IRB review. Livers were graded for steatosis, inflammation, and fibrosis by a pathologist using a double-blinded method and identified as ALD or normal. Primary human HSCs were purified from livers using pronase perfusion and gradient centrifugation method.

## METHOD DETAILS

### Isolation of primary hepatocytes

Primary hepatocytes were isolated as described previously (Li et al., 2016; Ying et al., 2017). Briefly, mice were infused with a calcium-free HEPES-phosphate buffer A (Calcium and magnesium-free PBS containing 0.2 μM EGTA, 10 mM HEPES, 1 mM glucose and 0.2% BSA, pH 7.4) via the vena cava for 3-5 min. After the color of the liver changed to a beige or light brown color, collagenase-containing buffer B (PBS with 1 mM magnesium and 1 mM calcium, 0.2% BSA, and 30 mM HEPES, 0.5mg/ml collagenase H) was perfused into the liver. After the appearance of cracking on the liver surface, perfusion was stopped and the liver was excised into ice-cold buffer A. Cells from digested livers were teased out, suspended in Buffer A, filtered through a 100 μm cell strainer, and centrifuged at 60 x g for 6 min at 4°C. The pellet was washed with Buffer B (no collagenase) twice and then mixed with Percoll (adjusted to physiological ionic strength with 10x PBS) to a final concentration of 36% and centrifuged at 100 x g for 10 min, 4°C. After removing the supernatant, the hepatocyte pellet was washed once with Buffer B (without collagenase) and then cultured in Williams Medium E containing 10% FBS on collagen-coated plates (GIBCO, Life Technologies) and antibiotics. After overnight incubation (16 hr), the culture medium was refreshed.

### Hepatic stellate cell (HSC) isolation

Mouse liver was sequentially perfused via the superior vena cava first with 30-40mL of calcium-free HEPES-phosphate buffer A, then with 0.5mg/mL pronase 30mL, and finally with 0.5 mg/mL collagenase D 30mL. After digestion of the clipped liver tissue in a mixture containing DNase of collagenase D and pronase for 20 minutes, the cell suspension was subjected to 50 x g centrifugation for 3 min to remove the residual liver parenchymal cells. The supernatant was collected and centrifuged at 900 x g for 8 min (4°C) to collect the non-parenchymal cells. The collected non-parenchymal cells were resuspended in 15% OptiPrep and transferred to a 15 mL centrifuge tube after sufficient mixing. Then, 5 mL of 11.5% OptiPrep and 2 mL of Gey's Balanced Salt Solution (GBSS; Sigma-Aldrich, St. Louis, MO) were individually layered onto the cell suspension. The tube was centrifuged at 2000 x g for 20 min (4°C, low acceleration), and the cell layer between the 11.5% OptiPrep and GBSS was collected. The obtained cells are purified HSCs. These cells were washed twice with centrifugation dilution solution (800 x g for 10 min, 4°C) and seeded with culture medium (10% FBS, 1% Glutax, and 2% penicillin/streptomycin) at 37°C.

### Co-culture assay

Kupffer cells (KCs) were seeded in the upper chamber of a trans-well plate (0.4 μm polycarbonate filter, Corning) and then transfected with miR-690 mimic or negative control mimic (5 pM/well). After 24hr, these KCs were co-cultured with NCD mouse hepatocytes at a ratio of 1:10, with hepatocytes placed in the lower chamber and KCs in the upper chamber for another 24hr. After 6hr fasting in serum-free medium, hepatocytes were stimulated with insulin (100 nM) for 15min and then collected for pAKT/AKT measurement.

### Hepatic Spheroid culture

Lean healthy 8-10 weeks old male mouse livers or healthy human livers were perfused with collagenase to prepare hepatocytes after 50xg centrifugation for 2 minutes and 100xg centrifugation for 10 minutes in 30% percoll suspension. The pellet was the source of hepatocytes. The supernatant, after 50xg centrifugation, was centrifuged at 1000xg for 20 minutes. The pellet was subjected to 10% Nycodenz gradient centrifugation at 2000xg for 20 minutes without brake. Stellate cell (SC) bands were collected from the top. The pellet was subjected to 20% percoll gradient centrifugation at 600xg for 15 minutes. The pellet was treated with red blood cell lysis buffer and centrifuged again at 400xg for 10 minutes. The resulting pellet is called non-parenchymal cells (NPCs). Spheroid composition: cells per well of 96-well ultra-low attachment plate Hep:SC:NPC=1600:400:600 Every 3rd day, 50% of the medium is replaced by serum free medium. Fibrogenesis is stimulated by a condition of fatty acids, fructose and LPS. Transfection with the miR-690 mimic (1 nM) started at day 6 and continued through days 9 and 12. Cultures are terminated at day 15 for RNA and protein analysis.

Please cite this article in press as: Gao et al., MiR-690 treatment causes decreased fibrosis and steatosis and restores specific Kupffer cell functions in NASH, Cell Metabolism (2022), https://doi.org/10.1016/j.cmet.2022.05.008





### Triglyceride detection

Triglyceride levels were detected using the Triglyceride Colorimetric Assay kit according to the manufacturer's instructions.

### Glucose tolerance (GTT) and insulin tolerance tests (ITT)

Glucose tolerance tests were performed by injecting mice intraperitoneally (i.p.) with dextrose (1 g/Kg body weight) after 16 h of fasting. After fasting mice for 6 h, insulin tolerance tests were performed by i.p. injection with insulin (0.35 or 0.175 units per kg of body weight for Western diet or NCD-fed mice, respectively).

### siRNA transfection

Recipient cells were treated with siRNA (20 pmol siRNA/0.1×$10^6$ cells) using the RNAiMAX reagent. Control cells were treated with a non-targeting control siRNA. The siRNAs were mixed with RNAiMAX reagent and then incubated for 15 min at room temperature. This mixture was then added to the cell media.

### miR-690 mimic transfection or *in vivo* treatment

The miR-690 mimic was transfected into recipient cells with the lipofectamine RNAiMAX reagent (ThermoFisher Scientific). After 24 hours, the transfection efficiencies were validated by qPCR analysis. For *in vivo* delivery, the miR-690 mimic or scrambled mimic were encapsulated with nanoparticles and then administrated into 16wks WD recipient WT mice (5 nmole mimic per mouse, twice per week) through tail vein injection.

### Immuno-fluorescence staining

Livers were snap frozen in optimum cutting temperature (O.C.T., Fisher Healthcare) with dry ice. Six μm cryo-sections of tissue sections were cut and fixed with pre-cold acetone for 20 min. Slides were blocked with 5% normal donkey serum for 60 min at RT. After washing, nuclei were stained with DAPI (4',6-Diamidino-2-28 phenylindole dihydrochloride) for 10min at room temperature. Mounting media and cover slips were then added to slides for imaging. Images were acquired on a Keyence Fluorescent Microscope, and were processed with ImageJ (NIH, Bethesda, MD).

### Quantitative Reverse Transcriptase-polymerase Chain Reaction (RT-PCR) Analysis

Total RNA was extracted using the RNA extraction protocol according to the manufacturer's instructions (Zymo Research). cDNA was synthesized using SuperScript III and random hexamers. qPCR was carried out in 10 μl reactions using iTaq SYBR Green supermix on a StepOnePlus Real-Time PCR Systems (ThermoFisher Scientific). For miRNA RT-PCR, cDNA was synthesized using TaqMan microRNA reverse transcription kit and miRNA primers (5x). qPCR was performed using TaqMan universal master mix II and miRNA primers (20x) in 10 μl reactions on a StepOnePlus Real-Time PCR Systems (ThermoFisher Scientific). The data presented correspond to the mean of $2^{-\Delta\Delta Ct}$ from at least three independent experiments after being normalized to β-actin or U6.

### Western blot analysis

Cells or tissues were homogenized in RIPA buffer supplemented with protease and phosphatase inhibitors. Equal amounts of cell lysate proteins (30 μg protein per lane for pAKT detection) from each biological replicate were subjected to western blotting. Using the ChemiDoc XRS imaging system (BioRad), the protein bands on blots were detected with the SuperSignal West Pico Chemiluminescent Substrate. Protein bands were analyzed using Image Lab software (BioRad). Western blot data in figures and supplemental figures are all representative of more than three independent experiments.

## QUANTIFICATION AND STATISTICAL ANALYSIS

Blinding was performed whenever deemed to be appropriate and applicable. Sample description and identification was unavailable to the core personnel during data plotting and analyses. No samples or data were excluded from the study for statistical purposes. Each *in vitro* experiment was independently performed in duplicate or triplicate to ensure reproducibility. Group sizes of 5 mice or greater were sufficient to reach a statistical power of at least 80%. Mice were assigned at random to treatment groups for all mouse studies. Tests used for statistical analyses are described in the figure legends. To assess whether the means of two groups are statistically different from each other, unpaired two-tailed Student's t test was used for statistical analyses, all data passed the normality test using Prism8 software (GraphPad software v8.0; Prism, La Jolla, CA). p values of 0.05 or less were considered to be statistically significant. Degrees of significance are indicated in the figure legends. For the results of glucose and insulin tolerance tests, statistical comparisons between the two groups at each time point were performed with unpaired two-tailed Student's t test.